Cosmic Ray Project

APPLIED PHYSICS LABORATORY

A DIVISION OF THE DEPARTMENT OF PHYSICS

UNIVERSITY OF WASHINGTON

The Zenith Angle Dependence of Cosmic

Ray Protons

TECHNICAL REPORT

APPLIED PHYSICS LABORATORY

UNIVERSITY OF WASHINGTON

A Division of the Department of Physics

THE ZENITH ANGLE DEPENDENCE OF COSMIC RAY PROTONS

By F. M. Charbonnier, W. R. Davis,
G. R. Garrison, J. E. Henderson,
C. E. Miller and W. M. Sandstrom*

TECHNICAL REPORT

OFFICE OF NAVY RESEARCH

CONTRACT N8onr 52008

Approved

J. E. Henderson, Director
Applied Physics Laboratory

ACKNOWLEDGEMENT

LIST OF TABLES

LIST OF FIGURES

THE ZENITH ANGLE DEPENDENCE OF COSMIC RAY PROTONS

CHAPTER I

INTRODUCTION

The composition and spectral distribution of the
cosmic radiation is a function of atmospheric depth, mag-
netic latitude and the direction of observation. Here one
refers, of course, to the total radiation. A complete
description of the radiation would give the intensity and
spectral composition of each class of particle as a function
of these parameters and the time. Such a complete descrip-
tion is not possible with present experimental techniques.
In successively refined experiments (1-7) conducted by this
laboratory, a technique of proton-meson analysis of the radi-
ation has been developed and the spectral composition of
these radiations studied at sea level and at 3.4 kilometers
altitude. These studies were all for radiation of vertical
incidence at the point of observation. It then became
desirable to undertake further observations in order to

find the change in composition and intensity with direction of observation at fixed atmospheric depth. Two programs of this kind have been carried out. In the work of Charbonnier (6), the spectral composition of the radiation of range greater than 15 cm. of lead was studied as a function of zenith angle. As was shown, the radiation defined in this way consists almost entirely of mu mesons. As a result of these measurements, it was possible to give a much more detailed experimental check of the theory of atmospheric development of the mu meson radiation than had been previously available. The present work reports a similar study of the radiation of range less than 15 cm. of lead. This radiation contains, in addition to low energy mesons, a large number of protons. Precautions taken to exclude the soft component are described in Chapter II, Section 1. In the past, of course, many studies of the zenith angle dependence of the total hard and soft components have been made. The present work is the first study of its kind for any part of the nucleonic radiation. As protons and mesons at lower altitudes are not thought to be closely related genetically, it was expected that quite different dependences on zenith angle would be found for the two types of radiation. As it turned out, the angular dependences of protons and mesons were found to be the same, within experimental error. As will be shown, this must be considered a fortuitous result

of the particular conditions of observation.

Charbonnier's observations on mesons were easily interpreted because of the almost complete lack of nuclear interaction of these particles. Their distribution as a function of depth and angle can be interpreted entirely in terms of the well understood processes of decay and energy loss by ionization. Such is not the case for protons or other particles showing strong nuclear interaction. Cross-sections are such that on the average a dozen or more colli-sions will have taken place between the top of the atmosphere and the point of observation of 3.4 kilometers. These colli-sions involve pi meson production along with production of secondary nucleons at large angles to the direction of the primary. The development of this radiation involves a cas-cade process qualitatively similar to that of the soft com-ponent. This has been discussed by Messel, Janossy and others (8-20). However, almost complete lack of either experimental or theoretical knowledge of cross-sections for the many processes involved causes the result to be one that can hardly be expected to be experimentally confirmed. In addition, a simplified one dimensional cascade has been considered so that the result cannot be compared with the present studies of angular dependence. It had been expected, because of the isotropy of the higher energy proton radiation plus the large angle scattering in successive nuclear collisions,

that the observed proton radiation at lower altitudes also would be almost isotropic. It was surprising to find that the intensity decreased by a factor of 3.2 in going from the vertical to a zenith angle of 45 degrees. This result in effect places an upper limit on the average deviation suffered in a nuclear collision. Rather than attempt a detailed cascade calculation based on questionable assumptions regarding cross-sections, a simplified phenomenological calculation has been made to give a description of the observed proton zenith angle dependence.

As a by-product of these observations, additional information on the proton spectrum has been obtained, as well as data on the meson zenith angle dependence for energies lower than those observed by Charbonnier.

CHAPTER II

THE EXPERIMENT

1. Experimental Arrangement

A sketch of the experimental arrangement is shown in
Figure I. The entire assembly may be rotated about a North-
South horizontal axis, perpendicular to the plane of the
figure, so that the cosmic ray beam at any zenith angle up
to 50° may be accepted. Anti-coincidence counters A1, which
lie outside the acceptance beam defined by counters C1 and
C2, serve to limit the number of cases in which shower events
are recorded. Only events of the type C1 + C2 - A1 - A2 -
A3 are recorded. A one-centimeter thick absorber in the form
of a half cylinder of lead placed above counter C2, plus the
absorber represented by the walls of the cloud chamber and
the coincidence counters establishes the minimum range and
momentum of accepted particles. The 15 centimeters of absorber
between C2 and A2 and 3, of course, determines the maximum
range accepted. As discussed by Todd (5), such range defin-
ition serves to resolve protons and mesons into distinct
momentum bands, in the absence of scattering and nuclear inter-
action. To the extent that these effects are ignored, then,
the apparatus accepts mesons of momentum 0.09 to 0.34 Bev/c,
and protons in the momentum band 0.4 to 1.0 Bev/c. In other
respects the apparatus is the same as that used by Garrison

(7). The inclusion of the one cm. absorber over C2 has removed a small overlap between the maximum meson momentum accepted and the minimum momentum of proton acceptance present in his experiment. This modification is not so large as to prevent comparison of present with previous work.

As shown in Figure I, anti-coincidence coverage below the 15 cm. of lead is quite complete. A double layer of counters has been used below the absorber to prevent particle leakage between the counters. Along the sides, a single layer was considered adequate, as in any case few particles will suffer such wide-angle scatterings. To prevent amplifier overloading from too high a counting rate, three anti-coincidence input amplifiers have been provided. One was fed from counters A1 while the tubes below the 15 cm. absorber were divided into two groups feeding the other two channels. The counter groups so defined could be separately scaled to detect defective counters.

As in previous work, the 2.5 cm. of lead absorber above A1 serve to insure recognition of electron showers. Such showers either actuate one of the counters A1, in which case the event is not recorded, or are recognized by their appearance in the chamber. This will be discussed later.

ACCEPTANCE BEAM

2.5 CM LEAD

A1

C1

MAGNET WINDING

DIAPHRAGM

CAMERA

CLOUD CHAMBER

POP VALVES

1 CM LEAD

A1

C2

5 CM LEAD

10 CM LEAD

A2 AND A3

1 FOOT
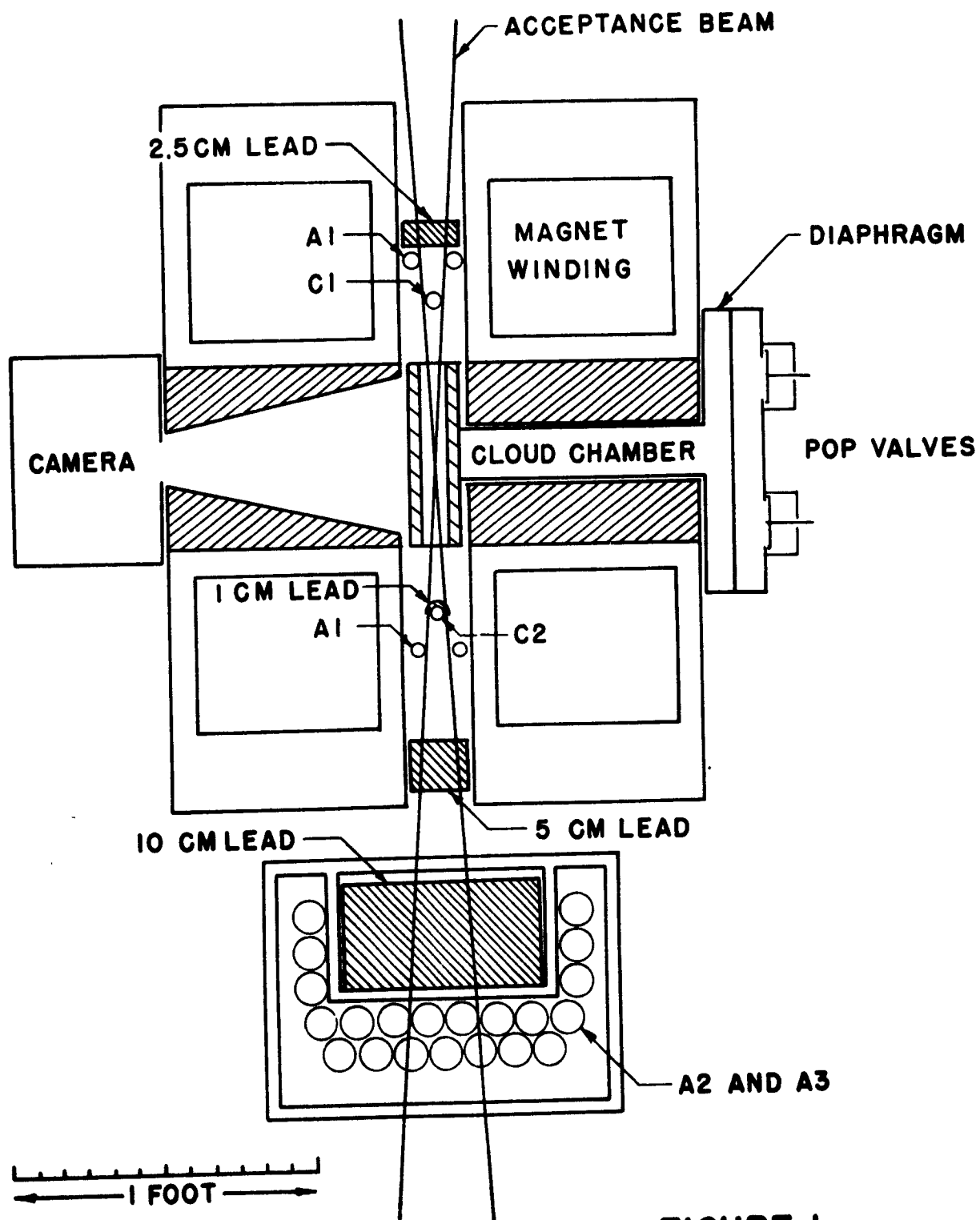
FIGURE 1
SKETCH OF THE
EXPERIMENTAL ARRANGEMENT

2. Experiments Performed

Three sets of measurements were taken with this apparatus located at Climax, Colorado, elevation 3.3 km. and magnetic latitude 48° North and in continuous 24-hour operation during the months of August, September, and October, 1951. Initial conjectures as to the results of the zenith angle measurements led to the conclusion that appreciable differences in intensity would require rather large angles of observation, so for this reason, an angle of 45° was chosen. The three sets differed only in the zenith angle to which the apparatus was tilted, a measurement being made at vertical incidence, at 45° to the East and 45° to the West of the zenith. Since the magnet could be tilted in only one direction with respect to the trailer in which it was installed, the trailer was oriented to give an East or West zenith angle. In each case, a reference structure on the magnet was made level in order to obtain the same amount of tilt East or West. The direction of tilt was changed periodically so that all data in a given direction were not obtained at once. Time did not permit the taking of data at more than one angle to the East and West plus the vertical.

For the vertical direction, a total of 3482 pictures was taken, of which 1387 were suitable for measurement according to the selection criteria to be described later. The West measurements provided 1126 measurable tracks out of a

total of 3962 pictures, the East 1304 out of 4488, for a total of 11,932 pictures. The magnetic field was reversed occasionally to indicate any asymmetry from this source. The data for vertical and East zenith angles are divided about equally between field direct and field reverse, but unfortunately the West data were all obtained with the field direct.

3. The Equipment

A brief description of the principal components of the equipment is included for the sake of completeness only, as their detailed description has appeared before (4,5,6,7). It should be mentioned that the use and constant improvement of this equipment by the above investigators during the three years preceding the date of this experiment was responsible for smooth, continuous, and dependable operation throughout the experiment.

Figure I shows the essential features of the magnet assembly. The cloud chamber proper is centered between the magnet poles, a conical hole in the forward pole providing access for photography, and a hole in the rear pole providing for a tube connecting the sensitive volume of the chamber with the expansion diaphragm at the rear. Illumination of the chamber was provided by four Sylvania type R4330 flash lamps, whose light was focused by cylindrical lenses into

the chamber, and by two 300-watt incandescent lamps for
visual inspection. These accessories, plus the necessary
Geiger counters and absorbers, were bolted to the inner face
of the rear magnet. The gap of $2\frac{1}{2}$ inches between the inner
magnet faces, where the sensitive volume of the chamber,
Geiger tubes, etc. were located, was maintained by steel
spacers at the right and left sides of the magnet. These
spacers also served to complete the magnetic circuit.

The chamber was filled with enough 60-40 n-propyl
alcohol-water mixture to saturate the volume, and finally
filled with argon to a total pressure of 20 pounds per
square inch above atmospheric. Expansion is accomplished
by releasing compressed air from behind a neoprene diaphragm
through two pop valves electrically connected in parallel.
The two pop valves provide faster air release than the single
pop valve used previously, while the electrically parallel
connection insures that the two valves open simultaneously.

The magnets provide a field of 8200 gauss with an
energizing current of 800 amperes, and are cooled by oil
flowing through the windings at a rate of 60 gallons per
minute. The oil in turn is cooled in an oil-water heat
exchanger. The cooling water was obtained from an artificial
lake whose constant head and temperature provided ideal
chamber operating conditions. Further temperature stabili-
zation was provided by a valve controlling a bypass on the

heat exchanger. Temperature drifts were detected by the unbalance in an AC bridge, one leg of which was immersed in the oil system. The error signal thus derived was then applied, through suitable circuits, to the task of opening and closing this valve. This system assured temperature stability to 0.01° Centigrade.

Appropriate electronic equipment provided for the following functions.

a. Event Selection. Simple twofold coincidence of resolving time 4 microseconds is obtained using a Rossi type coincidence circuit. Its output is delayed by a 5 microsecond univibrator whose output feeds a second Rossi circuit in which anti-coincidence mixing occurs. An anti-coincidence pulse of ten microseconds duration then arrives at the mixer five microseconds ahead of the coincidence pulse, thus blocking its further progress. The anti-coincidence circuit has the desirable feature of being continuously retriggerable. Thus, anti-coincidence blanking persists for ten microseconds after the last pulse received, no matter how frequently they arrive.

b. Programming. This unit contains power supplies including Geiger voltage, a scale of 16, with which each channel of the event selector, as well as the output of the anti-coincidence train, can be separately scaled, and mechanical registers for recording the C and C-A events.

c. Cloud Chamber Control. The desired event, selected
by the event selector, and recorded by the program unit, then
triggers this unit, which carries out the following sequence
of operations:

1. Expands the chamber

2. Removes the clearing field voltage

3. Records the expansion

4. After a time delay of 0.06 seconds to allow time
   for droplet growth, fires the flash lamps

5. Recompresses the chamber and reapplies the clearing
   field voltage

6. Provides circuit sterilization for a period of 90
   seconds to allow time for the chamber to recover

7. Moves the film to the next frame

8. Monitors all supply voltages

9. Provides for manual operation of the chamber and
   camera rewind, and sterilization to avoid the
   recording of spurious data, e.g., in the event
   of failure of the magnetic field.

CHAPTER III

CURVATURE MEASUREMENTS AND THE DETERMINATION OF
ABSOLUTE RATES

The determination of momentum of a particle is accomplished by measuring the radius of curvature of the track and applying the formula:

$$p = 3Br \times 10^{-5}$$

where p is momentum in Bev/c, B is the magnetic induction in gauss, and r is the radius of curvature in meters. With a magnetic field of 8200 gauss as used, p = r/4. Curvature measurements of nearly 4000 tracks required a compromise between inaccuracy and the consumption of time. The method used involves the comparison of the curvature of a track whose image is projected on the screen of a comparator, with that of a standard arc. The process whereby these arcs were prepared and a complete description of the measurement technique have been presented in previous work (4,5). More recently, the optical system of the comparator underwent an overhaul, and the magnetic field reversals mentioned in Chapter II, section 2, were performed to disclose any curvature distortion introduced by the overhaul. The data presented here, consisting only of low momentum particles,

14

showed no such effect. However, the succeeding experiment by Charbonnier (6), in which high energy mesons were accepted, was far more sensitive to such an error and did indeed reveal the presence of one. Both the source and correction of this fault have been explained exhaustively by Charbonnier. The error amounts to introduction of an additional spurious curvature of 1/40 reciprocal meters in such a way as to increase the curvature of tracks appearing convex upwards in the comparator. As described by the above authors, the preparation of the standard arcs precisely cancels out the error for tracks of this particular kind. For tracks of the opposite sign of curvature, however, the compensating error inherent in the standard arcs no longer compensates, but actually accentuates the discrepancy to the extent of 1/20 reciprocal meters, i.e., twice the distortion. Hence, the tracks appearing convex downwards in the comparator, and these include negative particles with the magnetic field direct and positive particles with the field reversed, must have their measurements corrected by this amount. In Charbonnier's case, this correction was necessary. In this case, it is relatively unimportant, but it is felt that the correction should be made because of the systematic nature of the error.

The apparatus used in this experiment does not record absolute rates. They can be inferred, however, provided we make several assumptions. An accurate record was kept of the

so-called C-A rate, which is the rate at which counters C1 and C2 provide simultaneous outputs (within 4 microseconds) unaccompanied by anti-coincidence counts. The cloud chamber does not respond to C A counts which occur during the 90 second sterilization period provided to allow thermal recovery of the chamber after each expansion. Neither does each C-A count represent a single particle traversing the telescope, since shower protection is not complete. Identity of the nature of the event causing the count is learned on examining the photographs, which are placed in one of the following three categories.

a. Single Tracks. Such a photograph is characterized by the appearance of a single track in such a direction as to indicate traversal of both C counters. The length of the track, as well as the occurrence of obviously pre- or post-expansion tracks is ignored.

b. Showers. These are photographs showing two or more time-coincident tracks.

c. Misses. Occasionally a photograph will show a completely empty chamber. This is also interpreted as a shower phenomenon.

It is assumed that the C-A counts occurring during the 90-second sterilization time represent the same statistical distribution of events as those photographed. This means that the single track rate can be computed from:

$$\text{Single Track Rate} = \frac{(\text{No. of Single Tracks})}{(\text{Total No. of Frames})} \text{ (C-A Rate)}$$

This single track rate then represents the total rate corrected for the 90-second recovery time and the occurrence of showers. The statistical uncertainty in this rate, as quoted in the data sheets, is the sum of the uncertainty in the C-A rate and the statistical uncertainty in the number of single tracks. However, not all single tracks are measured, since we have assumed that tracks whose length does not exceed 70% of the chamber diameter cannot be measured accurately. As compared with straight tracks, this criterion discriminates against curved tracks to the extent of about 3% at the lowest momentum measured (0.09 Bev/c). Above .25 Bev/c the discrimination is negligible. Thus we compute.

Number of Single Tracks of Momentum p in dp per unit time

$$= \frac{(\text{Number of Measured Tracks of mom. p in dp})}{(\text{Total Number of Measured Tracks})} \text{ (Single Track Rate)}$$

If we divide this quantity by the product of the area of and solid angle subtended by the telescope, herein called the aperture, and the width of the momentum interval, dp, we arrive at the absolute rate in particles per Bev/c cm^2 sterad hour. If we use the formula on page 13, p = r/4, then dp = dr/4. For convenience, a normalization factor can be defined for each set of data:

$$\text{Normalization Factor} = \frac{(\text{Single Track Rate})(4)}{(\text{Total Number of Measured Tracks}) \times (\text{Aperture})}$$

Thus:

$$\text{Absolute Intensity} = \frac{\text{(No. of Tracks of Mom. p in dp)} \times \text{(Normalization Factor)}}{\text{(Radius Interval)}}$$

The only ill-defined quantity included above is the aperture of the telescope. Its uncertainty traces to the uncertainty in the sensitive volume of the Geiger tubes. From the size and separation of the counters, this coverage was estimated to be about 1 cm^2 steradian, a figure later corrected to 0.94 (6) by comparison with the very accurate determination of the vertical intensity made by Greisen as quoted by Rossi (25).

CHAPTER IV

DATA

Analysis of the data from the three sets of measurements appears in Tables I - III. The direction of the magnetic field was reversed occasionally for the purpose of detecting the presence of any systematic curvature distortion. As mentioned in Chapter III, such a distortion is present, necessitating separate treatment for the two kinds of data, field direct and field reverse. In the 45° West case, only one direction of field was used, so that here no separate treatment is necessary.

Listed in the tables are the total number of frames inspected and the number of frames containing showers, misses and single tracks respectively. The number of frames containing single tracks whose length exceeds the lower limit of 70% of the chamber diameter is listed as "Total Measured." The latter are further broken down into positive, negative, and "infinite, no sign," these latter being in the measurable class, i.e., long enough, but of such small curvature that no definite assignment of sign could be made.

In one case (45° East, field direct), chamber operation was so poor for a short period that accurate measurements were impossible. However, the tracks photographed during this short time were inspected and classified as to type of event

(single track, shower or miss, positive or negative). Thus, the figures for these classifications in Table II include these data, but the total measured entry and the tabulated momentum spectra do not. The inclusion increases the statistical accuracy of the quoted rates and hence (but only indirectly) the accuracy of the spectra. The normalization factor and the various rates have already been explained in the chapter on determination of rates. Finally, the tabulated momentum spectra appear. The various entries are connected by the following formula:

$$\text{Absolute Intensity} = \left(\frac{\text{No. of Particles}}{\text{Radius Interval}}\right) (\text{Norm. Factor})$$

$$\pm \frac{(\text{Abs. Intensity})}{(\text{No. of Particles})^{\frac{1}{2}}}$$

TABLE I   VERTICAL CASE

Direction of Observation: Vertical
Magnetic Latitude.   48° North
Altitude   3.3 Kilometers

FIELD DIRECT DATA

Positives	655	Total Frames	2792
Negatives	252	Average Yield of	
Infinites, No Sign	3	Single Tracks	41%
Total Measured	910	C-A Rate per Hour	27.5 ± 0.4
Total Single Tracks	1142	Single Track Rate	11.3 ± 0.4
Running Time	173.33 hrs	Normalization	
C-A Counts	4752	Factor	0.0495

Positives

Letter Group	Number of Particles	Radius Interval meters	Average Momentum Bev/c	Absolute Intensity particles per Bev/c cm^2 sterad hour
O-A	11	0.316	0.048	1.7 ± 0.6
A-E	57	0.345	0.120	8.2 ± 1.1
E-I	89	0.429	0.213	10.3 ± 1.1
I-L	92	0.470	0.322	9.7 ± 1.0
L-N	42	0.380	0.425	5.5 ± 0.9
N-P	69	0.480	0.530	7.1 ± 0.9
P-R	83	0.660	0.665	6.2 ± 0.7
R-T	82	0.980	0.865	4.1 ± 0.5
T-V	61	1.790	1.200	1.7 ± 0.25
V-X	47	4.150	1.920	0.6 ± 0.09
X-	22	--		

Negatives

Letter Group	Number of Particles	Radius Interval meters	Average Momentum Bev/c	Absolute Intensity particles per Bev/c cm^2 sterad hour
O-A	11	0.312	0.048	1.7 ± 0.6
A-E	47	0.330	0.116	7.1 ± 1.0
E-I	88	0.390	0.200	11.2 ± 1.1
I-L	71	0.420	0.300	8.4 ± 1.0
L-N	13	0.320	0.390	2.0 ± 0.6
N-P	2	0.390	0.475	0.25 ± 0.1
P-R	3	0.510	0.585	-- --
R-T	4	0.710	0.730	-- --
T-V	4	1.140	0.955	-- --
V-X	4	2.150	1.350	-- --
X-	5	13.330	--	-- --

TABLE I (continued)

FIELD REVERSE DATA

Positives	326	Average Yield of	
Negatives	148	Single Tracks	45%
Infinite, No Sign	3	C-A Rate per Hour	29.1 ± 0.6
Total Measured	477	Single Track Rate	13.1 ± 0.9
Total Single Tracks	637	Normalization	
Total Frames	1404	Factor	0.110
Running Time	82.64 hrs		
C-A Counts	2404		

Positives

Letter Group	Number of Particles	Radius Interval meters	Average Momentum Bev/c	Absolute Intensity particles per Bev/c $\hat{c}m^2$ sterad hour
O-A	9	0.312	0.048	
A-E	23	0.330	0.116	3.2 ± 1.0
E-I	44	0.390	0.200	7.7 ± 1.6
I-L	55	0.420	0.300	12.4 ± 1.9
L-N	29	0.320	0.390	14.4 ± 1.9
N-P	31	0.390	0.475	10.0 ± 1.9
P-R	31	0.510	0.585	8.8 ± 1.6
R-T	43	0.710	0.730	6.7 ± 1.2
T-V	31	1.140	0.955	6.7 ± 1.0
V-X	22	2.150	1.350	3.0 ± 0.5
X-	8	13.330	--	1.1 ± 0.3
				-- --

Negatives

Letter Group	Number of Particles	Radius Interval meters	Average Momentum Bev/c	Absolute Intensity particles per Bev/c $\hat{c}m^2$ sterad hour
O-A	4	0.316	0.048	
A-E	27	0.345	0.120	1.4 ± 0.7
E-I	43	0.429	0.213	8.6 ± 1.7
I-L	42	0.470	0.322	11.0 ± 1.7
L-N	12	0.380	0.425	9.8 ± 1.5
N-P	5	0.480	0.530	3.5 ± 1.0
P-R	2	0.660	0.665	1.2 ± 0.6
R-T	2	0.980	0.865	0.3 ± 0.2
T-V	4	1.790	1.200	--
V-X	1	4.150	1.920	--
X-	6	--	--	--

TABLE II   EAST CASE

Direction of Observation: 45° East of Vertical
Magnetic Latitude: 48° North
Altitude: 3.3 Kilometers

FIELD DIRECT DATA

Positives	416	Average Yield of	
Negatives	240	Single Tracks	36.5%
Infinite, No Sign	3	C-A Rate per Hour	10.1 ± 0.2
Total Measured	533	Single Track Rate	3.7 ± 0.2
Total Single Tracks	767	Normalization	
Total Frames	2099	Factor	0.0278
Running Time	287.85 hrs		
C-A Counts	2894		

Positives

Letter Group	Number of Particles	Radius Interval meters	Average Momentum Bev/c	Absolute Intensity particles per Bev/c cm^2 sterad hour
O-A	4	0.316	0.048	0.35 ± 0.2
A-E	25	0.345	0.120	2.1 ± 0.4
E-I	39	0.429	0.213	2.5 ± 0.4
I-L	51	0.470	0.322	3.0 ± 0.4
L-N	18	0.380	0.425	1.3 ± 0.3
N-P	37	0.480	0.530	2.1 ± 0.35
P-R	39	0.660	0.665	1.6 ± 0.3
R-T	46	0.980	0.865	1.3 ± 0.2
T-V	34	1.790	1.200	0.5 ± 0.09
V-X	26	4.150	1.920	0.2 ± 0.03
X-	14	--	--	-- --

Negatives

Letter Group	Number of Particles	Radius Interval meters	Average Momentum Bev/c	Absolute Intensity particles per Bev/c cm^2 sterad hour
O-A	5	0.312	0.048	0.45 ± 0.2
A-E	35	0.330	0.116	2.9 ± 0.5
E-I	80	0.390	0.200	5.7 ± 0.7
I-L	59	0.420	0.300	3.9 ± 0.5
L-N	6	0.320	0.390	0.5 ± 0.2
N-P	2	0.390	0.475	0.14 ± 0.1
P-R	2	0.510	0.585	0.1 ± 0.07
R-T	-	0.710	0.730	-
T-V	-	1.140	0.955	-
V-X	-	2.150	1.350	-
X-	-	13.330	--	-

TABLE II (continued)

FIELD REVERSE DATA

Positives	404	Average Yield	33.4%
Negatives	238	of Single Tracks	
Infinite, No Sign	3	C-A Rate per Hour	9.48 + 0.15
Total Measured	645	Single Track Rate	3.06 ∓ 0.15
Total Single Tracks	795	Normalization	
Total Frames	2378	Factor	
Running Time	379.87 hrs		0.0190
C-A Counts	3602		

Positives

Letter Group	Number of Particles	Radius Interval meters	Average Momentum Bev/c	Absolute Intensity particles per Bev/c cm^2 sterad hour
O-A	5	0.312	0.048	
A-E	27	0.330	0.116	0.3 + 0.2
E-I	70	0.390	0.200	1.6 ∓ 0.3
I-L	70	0.420	0.300	3.4 ∓ 0.4
L-N	48	0.320	0.390	3.2 ∓ 0.4
N-P	58	0.390	0.475	2.8 ∓ 0.4
P-R	56	0.510	0.585	2.8 ∓ 0.4
R-T	35	0.710	0.730	2.1 ∓ 0.3
T-V	18	1.140	0.955	0.9 ∓ 0.15
V-X	11	2.150	1.350	0.3 ∓ 0.07
X-	3	13.330	--	0.09 ∓ 0.05
				--

Negatives

Letter Group	Number of Particles	Radius Interval meters	Average Momentum Bev/c	Absolute Intensity particles per Bev/c cm^2 sterad hour
O-A	3	0.316	0.048	
A-E	49	0.345	0.120	0.18 + 0.1
E-I	71	0.429	0.213	2.7 ∓ 0.4
I-L	63	0.470	0.322	3.1 + 0.4
L-N	26	0.380	0.425	2.5 ∓ 0.35
N-P	8	0.480	0.530	1.3 + 0.3
P-R	7	0.660	0.665	0.3 ∓ 0.1
R-T	4	0.980	0.865	0.2 ∓ 0.08
T-V	2	1.790	1.200	0.08 ∓ 0.04
V-X	4	4.150	1.920	--
X-	2	--	--	--
				--

TABLE III   WEST CASE

Direction of Observation: 45° West of Vertical
Magnetic Latitude: 48° North
Altitude: 3.3 Kilometers

(All data with field direct)

Positives	775	Average Yield of	
Negatives	336	Single Tracks	35%
Infinite, No Sign	16	C-A Rate per Hour	10.9 + 0.2
Total Measured	1127	Single Track Rate	3.8 ∓ 0.2
Total Single Tracks	1338	Normalization	
Total Frames	3835	Factor	0.0135
Running Time	508.70 hrs		
C-A Counts	5538		

Positives

Letter Group	Number of Particles	Radius Interval meters	Average Momentum Bev/c	Absolute Intensity particles per Bev/c cm² sterad hour
O-A	14	0.316	0.048	0.6 + 0.16
A-E	54	0.345	0.120	2.1 ∓ 0.3
E-I	101	0.429	0.213	3.2 + 0.3
I-L	109	0.470	0.322	3.1 + 0.3
L-N	63	0.380	0.425	2.2 + 0.3
N-P	57	0.480	0.530	1.6 + 0.2
P-R	90	0.660	0.665	1.8 + 0.2
R-T	96	0.980	0.865	1.3 + 0.15
T-V	78	1.790	1.200	0.6 ∓ 0.1
V-X	65	4.150	1.920	0.2 ∓ 0.03
X-	31	--	--	- -

Negatives

Letter Group	Number of Particles	Radius Interval meters	Average Momentum Bev/c	Absolute Intensity particles per Bev/c cm² sterad hour
O-A	12	0.312	0.048	0.5 + 0.15
A-E	66	0.330	0.116	2.7 ∓ 0.35
E-I	108	0.390	0.200	3.7 ∓ 0.40
I-L	96	0.420	0.300	3.1 ∓ 0.30
L-N	15	0.320	0.390	0.6 ∓ 0.20
N-P	8	0.390	0.475	0.3 ∓ 0.1
P-R	7	0.510	0.585	0.2 ∓ 0.1
R-T	4	0.710	0.730	- -
T-V	4	1.140	0.955	- -
V-X	11	2.150	1.350	- -
X-	9	13.330	--	- -

TABLE IV   COMBINED VERTICAL DATA 1950-1951

Direction of Observation: Vertical
Magnetic Latitude: 48° North
Altitude: 3.3 Kilometers

Positives	2666	Average Yield of	
Negatives	1052	Single Tracks	48.7%
Infinite, No Sign	31	C-A Rate per Hour	24.8 ± 0.17
Total Measured	3749	Single Track Rate	12.1 ± 0.25
Total Single Tracks	5126	Normalization	
Total Frames	10521	Factor	0.0129
Running Time	833.02 hrs		
C-A Counts	19,878		

Positives

Letter Group	Number of Particles	Radius Interval meters	Average Momentum Bev/c	Absolute Intensity particles per Bev/c cm² sterad hour
O-A	52	0.316	0.048	2.1 ± 0.3
A-E	199	0.345	0.120	7.4 ± 0.6
E-I	321	0.429	0.213	9.7 ± 0.6
I-L	419	0.470	0.322	11.5 ± 0.6
L-N	189	0.380	0.425	6.4 ± 0.5
N-P	252	0.480	0.530	6.8 ± 0.5
P-R	309	0.660	0.665	6.0 ± 0.4
R-T	331	0.980	0.865	4.4 ± 0.3
T-V	235	1.790	1.200	1.7 ± 0.1
V-X	193	4.150	1.920	0.6 ± 0.05
X-	166	--	--	- -

Negatives

Letter Group	Number of Particles	Radius Interval meters	Average Momentum Bev/c	Absolute Intensity particles per Bev/c cm² sterad hour
O-A	49	0.316	0.048	2.0 ± 0.3
A-E	189	0.345	0.120	7.1 ± 0.6
E-I	332	0.429	0.213	10.0 ± 0.6
I-L	286	0.470	0.322	7.9 ± 0.5
L-N	62	0.380	0.425	2.1 ± 0.3
N-P	25	0.480	0.530	0.7 ± 0.2
P-R	17	0.660	0.665	0.3 ± 0.09
R-T	18	0.980	0.865	0.2 ± 0.06
T-V	16	1.790	1.200	0.1 ± 0.03
V-X	21	4.150	1.920	0.07 ± 0.02
X-	37	--	--	-- --

CHAPTER V

DISCUSSION OF THE RESULTS

For the vertical case, data of a similar nature had
been obtained previously in studying the form of the proton
spectrum (7). Nevertheless, observations for this direction
were repeated, in part because of alteration of the equipment
(Chapter II, Section 1) and in part as a check on the previous
work, and because it was felt best that for comparison between
the various directions of observation, the data should be
taken in close succession rather than a year apart. The
present and previous spectra for the vertical case agree well
within statistics, a fact that is regarded as proof that the
equipment had undergone no change in performance during the
intervening year. For improved statistics, the two sets of
data have been combined with the result shown in Figure VI.

An explanation of the difference in form of the spectra
for positive and negative particles has been given previously
in connection with the determination of the proton spectrum
(7). It should be mentioned here that the negative distribu-
tion contains mu mesons only, while the positive distribution
is for positive mu mesons plus protons. While the total
intensity of positive mesons is known to exceed that of the
negative by some 20%, at momenta above 0.5 Bev/c where the
selection method excludes almost all mesons the difference

between the positive and negative intensities can be taken as a measure of the proton intensity.

1. The Meson Spectrum

In Figures II to V the vertical, the 45° East, and the 45° West spectra are given, along with the 45° spectrum averaged over East and West The latter spectrum, Figure V, is represented by plotted points only, the curves appearing on the figure for comparison purposes being the combined vertical data of Figure VI. The plotted points are the measured rates multiplied by a scale factor of 3.2 to allow comparison of the spectral shapes. With this multiplication factor and within statistics, the average East-West spectrum and the vertical spectrum do not differ. This is true for both the proton and meson radiation. An explanation of the zenith angle dependence of the meson radiation has been given in Charbonnier's study of this component. It was surprising to find the same zenith angle dependence for protons as for mesons since the two types of particles are not thought to be closely related genetically at this altitude. It should also be pointed out that the East and West spectra agree between themselves within statistics. This is shown in Figure VII. Thus, within the accuracy of the present observations, neither protons nor mesons at this altitude show any East-West asymmetry. The observed agreement in the zenith angle dependence of protons and mesons is

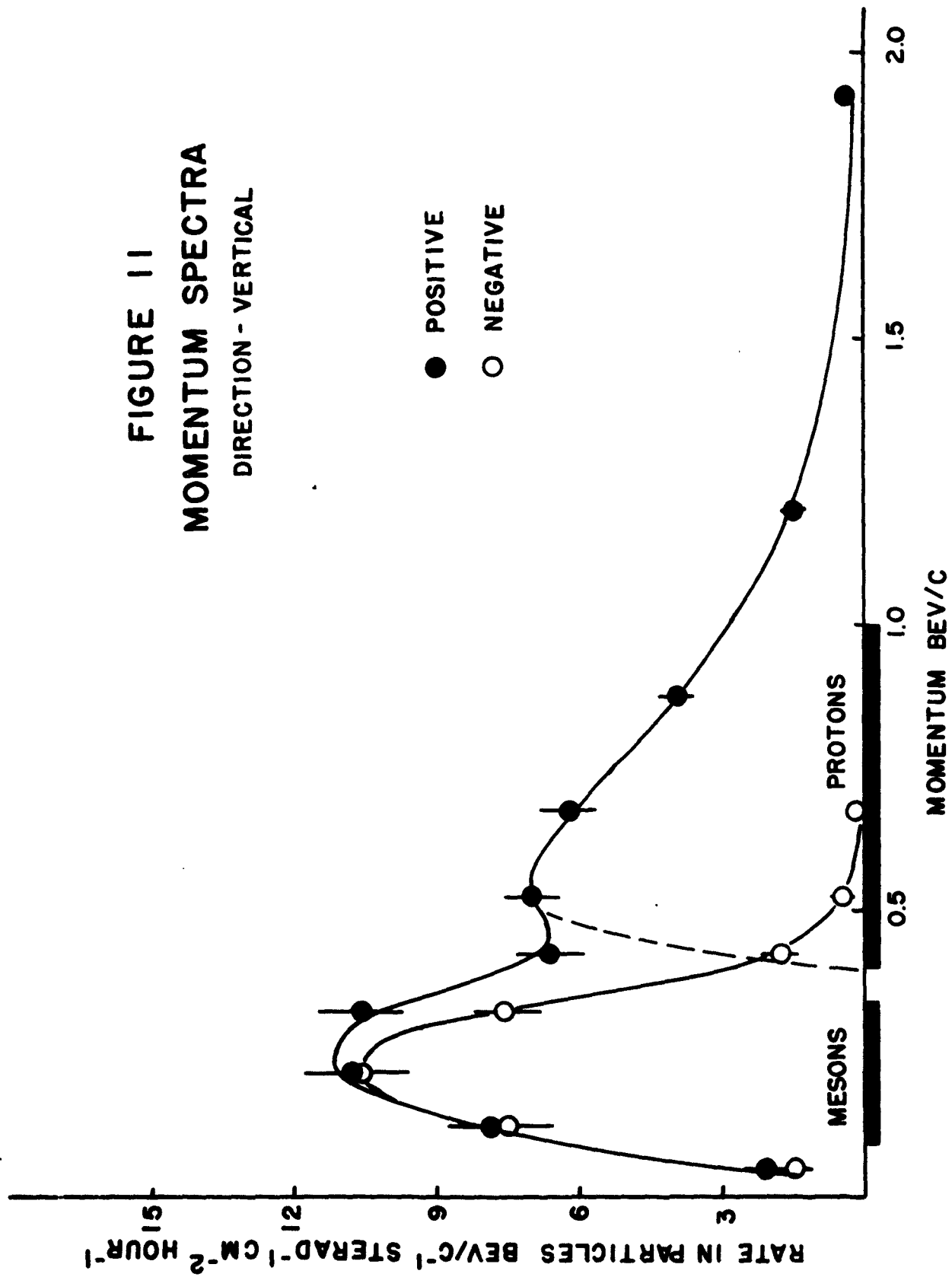FIGURE 11
MOMENTUM SPECTRA
DIRECTION - VERTICAL

● POSITIVE
○ NEGATIVE

PROTONS

MESONS

MOMENTUM BEV/C

RATE IN PARTICLES BEV/C⁻¹ STERAD⁻¹ CM⁻² HOUR⁻¹

FIGURE III
MOMENTUM SPECTRA
DIRECTION - 45° EAST

● POSITIVES
○ NEGATIVES

MOMENTUM BEV/C

RATE IN PARTICLES BEV/C⁻¹ STERAD⁻¹ CM⁻² HOUR⁻¹
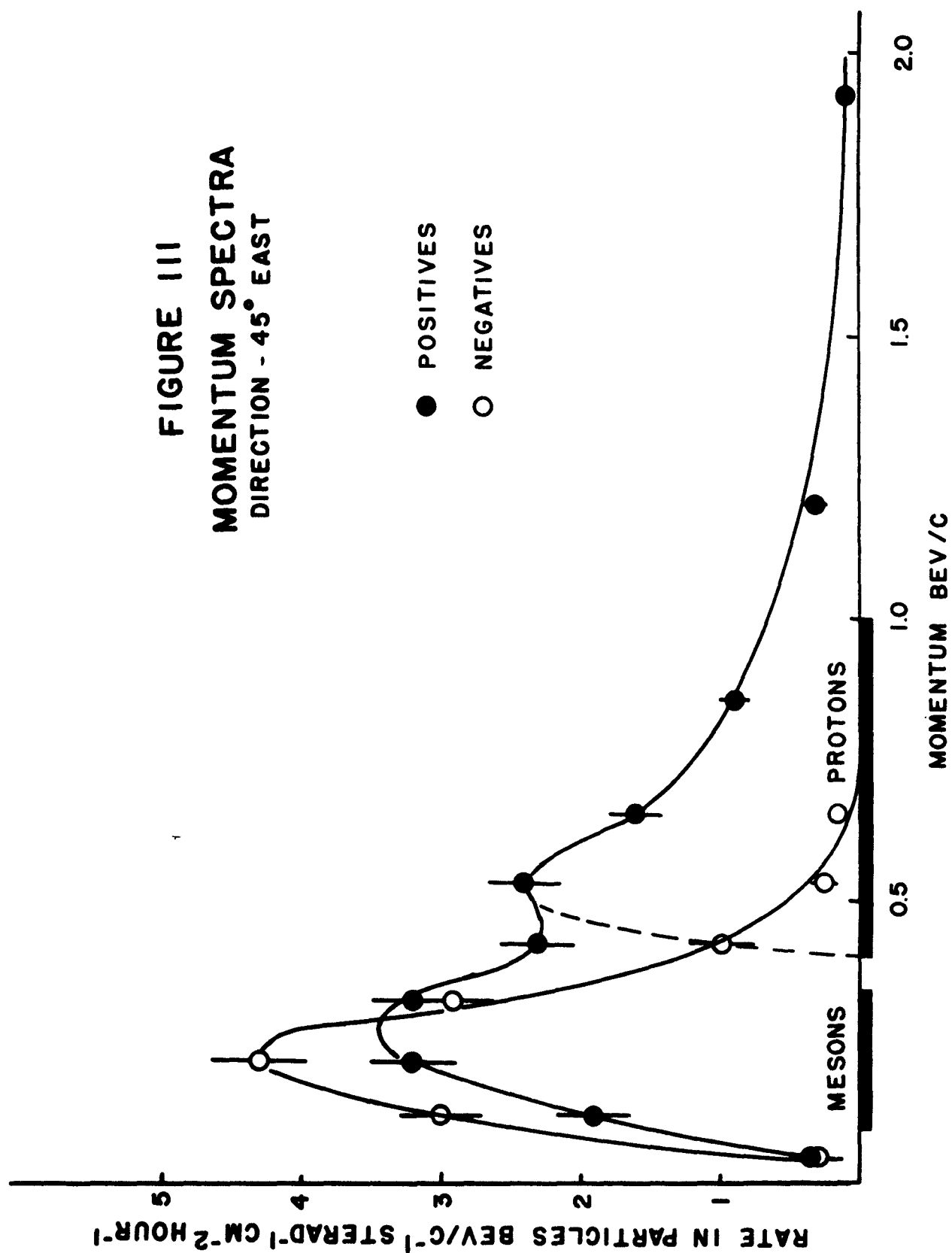
FIGURE IV
MOMENTUM SPECTRA
DIRECTION -45° WEST

● POSITIVE
○ NEGATIVE

MOMENTUM BEV/C

RATE IN PARTICLES BEV/C⁻¹ STERAD⁻¹ CM⁻² HOUR⁻¹
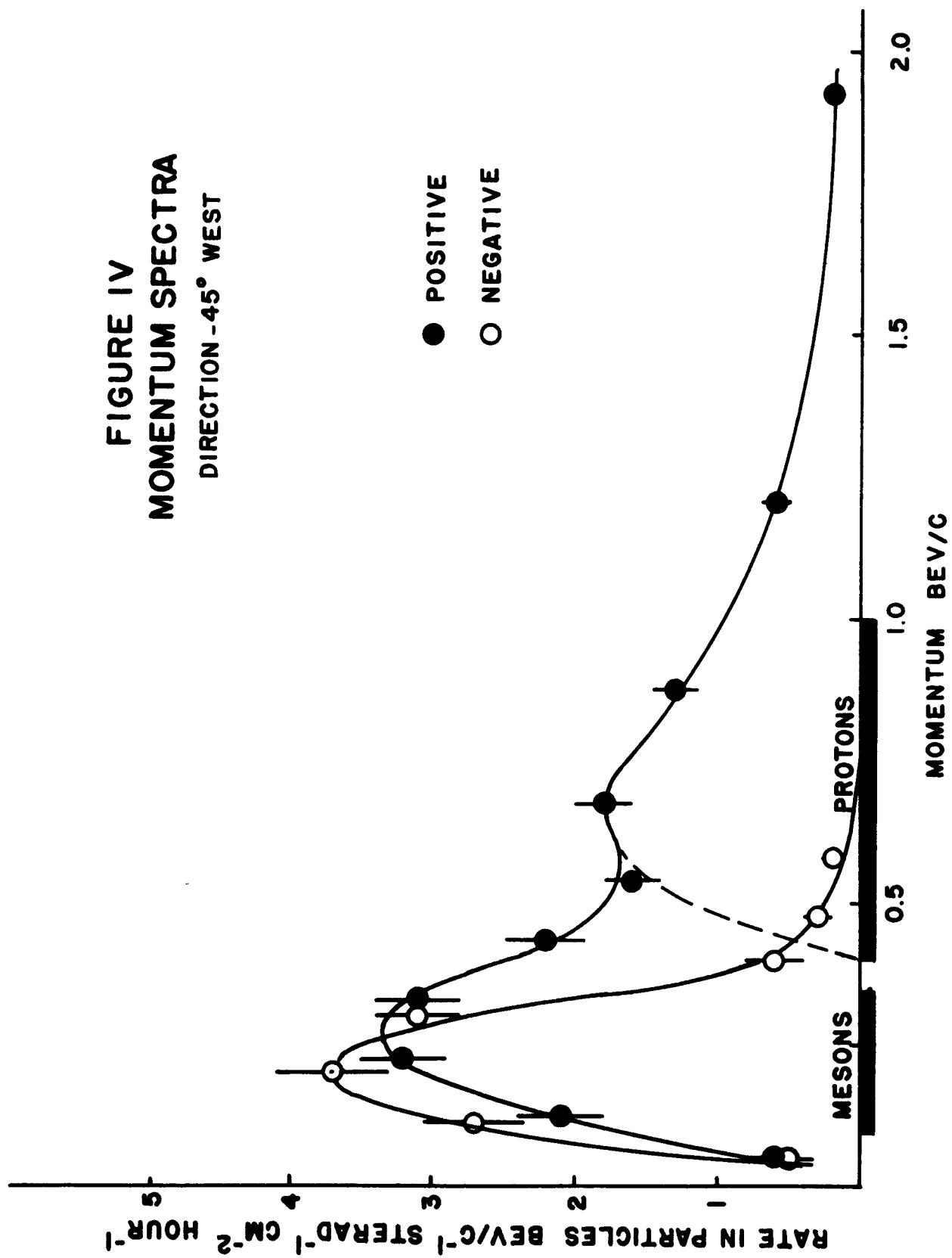
FIGURE V
COMPARISON OF
MOMENTUM SPECTRA
POINTS PLOTTED ARE FOR THE 45°
POSITIVE SPECTRUM AVERAGED OVER
EAST AND WEST, AND MULTIPLIED BY
A FACTOR 3.2
CURVE DRAWN IN IS THE COMBINED
VERTICAL POSITIVE SPECTRUM

RATE IN PARTICLES BEV/c⁻¹ CM⁻² STERAD⁻¹ HOUR⁻¹

MOMENTUM BEV/C
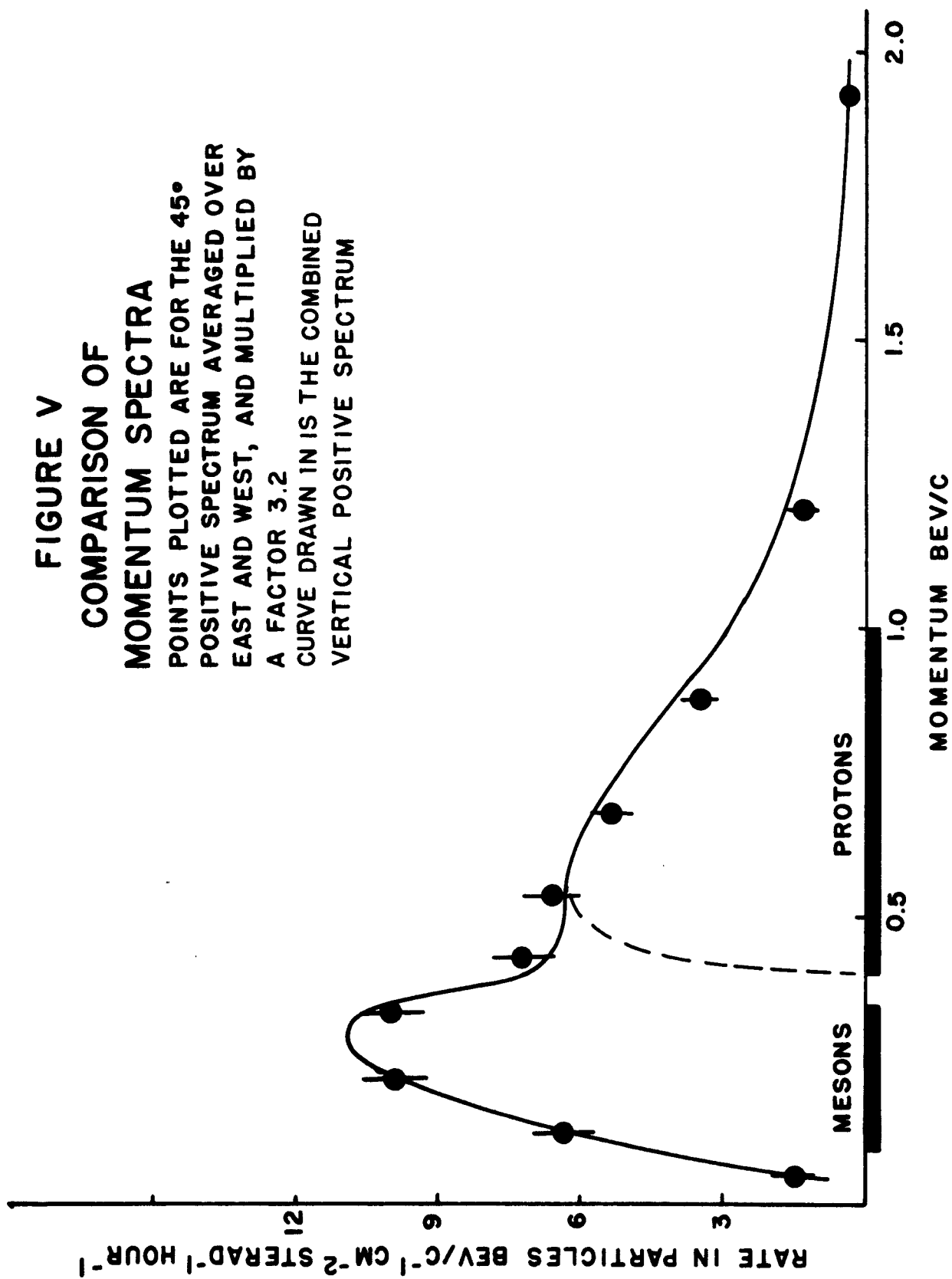
FIGURE VI
MOMENTUM SPECTRA
COMBINED VERTICAL DATA '50-'51
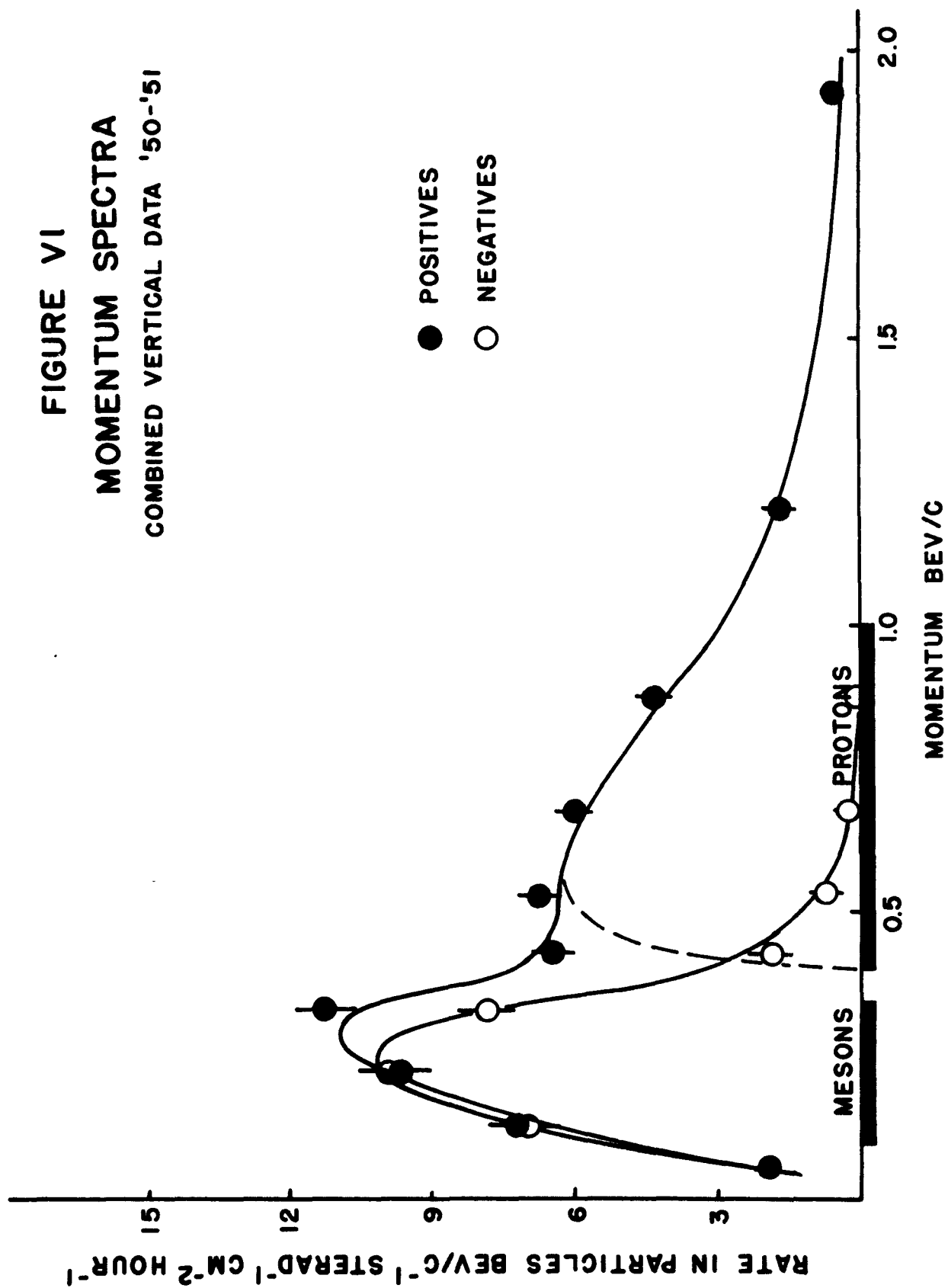
FIGURE VII
MOMENTUM SPECTRA
CURVES ARE AVERAGED E-W DATA
POINTS ARE AS FOLLOWS:

● POSITIVE 45° E
○ NEGATIVE 45° E
◐ POSITIVE 45° W
◑ NEGATIVE 45° W

MOMENTUM BEV/C

RATE IN PARTICLES BEV/C⁻¹ STERAD⁻¹ CM⁻² HOUR⁻¹

PROTONS
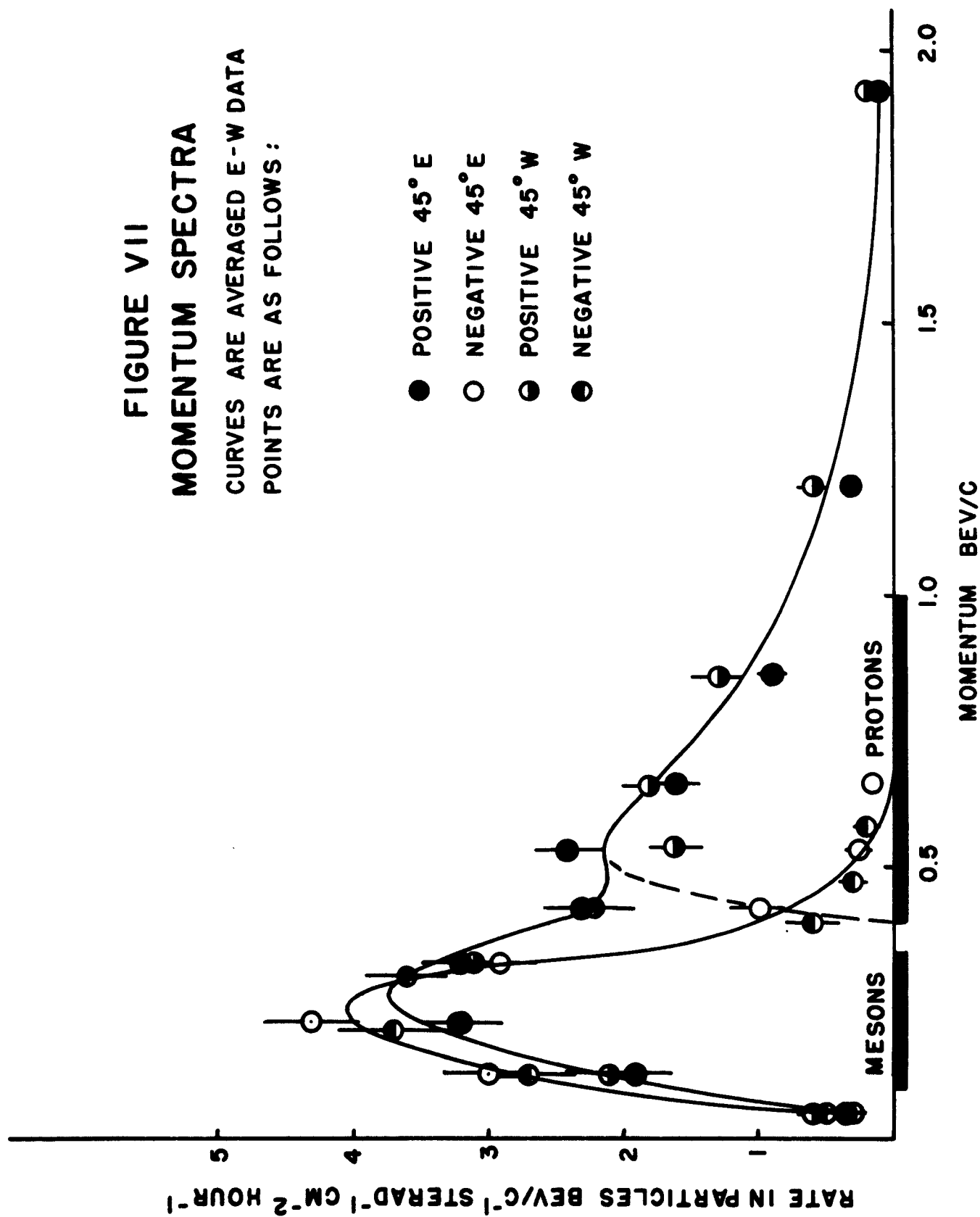
MESONS

considered to be fortuitous. Thus while the meson intensity decreases by a factor of 3.2 from zero to 45 degrees for the low momentum mesons observed here, this ratio does not hold at higher energies. At 2 Bev/c, the intensity ratio for mesons is found to be about 2 (6).

It is not the primary purpose of this experiment to explain the behavior of mesons. The zenith angle dependence of these particles has been thoroughly discussed by Charbonnier (7). One assumes that essentially all mesons observed at lower altitudes are produced isotropically at great atmospheric heights. Taking into account the negligible scattering of these particles, their radioactive decay and ionization energy loss in traversing the atmosphere, one accounts quantitatively for the observed intensity and directional distribution at lower altitudes. With these assumptions, a transformation can be found relating the vertical and 45° spectra at lower altitudes. In this way, from the observed vertical intensity at 3.3 km. for a momentum of 0.8 Bev/c one predicts a 45° intensity of 6.0 $\pm$ .3 particles/Bev/c cm^2 sterad hour, at 0.25 Bev/c. The 45° intensity at 0.25 Bev/c observed in the present work is 7.19 $\pm$ 0.33. Agreement between the predicted and observed values is not considered too bad, although outside the limits of statistical accuracy. Charbonnier did not observe meson intensities at momenta below 0.5 Bev/c. The predictions of a 45° intensity at 0.25

Bev/c was nevertheless made since this depends on his observed intensity at 0.8 Bev/c. At this low residual momentum, because of the increased importance of scattering, the computation is not expected to have comparable validity with Charbonnier's results at higher momenta. As the radiation intensity decreases with increasing zenith angle, the net effect of scattering will be to increase the intensity at large zenith angles at the expense of the intensity at smaller angles. This is in the direction of the observed and predicted intensities.

2. The Proton Spectrum

As compared to the meson radiation, the atmospheric development of the proton radiation (and the nucleonic radiation in general) is greatly complicated by nuclear interaction which here becomes the most important single process. Development of the nucleonic radiation involves a cascade process qualitatively similar to that of the soft component. The cascade is propagated through the atmosphere principally by protons and neutrons (22-24) produced in successive penetrating showers. Pi mesons originating in these showers decay too quickly to have high probability of undergoing further nuclear interactions while the mu mesons secondary to them do not undergo appreciable nuclear interaction at all, and so take no part in further propagation of the

cascade. Compared to the electromagnetic cascade, the interaction path lengths here are in the order of 100 g/cm^2, instead of the few g/cm^2 characterizing the radiation lengths of the electron cascade. The nucleonic cascade had been discussed in detail in a number of papers by Heitler, Janossy and Messel (8-20). The treatment there is phenomenological in regard to the form assumed for the nuclear cross-section. With this exception the mathematical treatment is complete with respect to fluctuations resulting from geometrical and statistical factors. The cross-section is assumed to be a function of the fractional energy loss of the primary, independent of the initial energy. The cross-sections employed do not include a description of the angular distribution of the secondary nucleons. Thus the zenith angle effects have not been computed, so that this treatment cannot be compared with the present experiment.

The constants in the cross-sections used by the above authors were so chosen as to conform to experimental values for the removal path length of the nucleonic radiation. Absorption of the radiation producing penetrating showers has been studied by Van Allen, Bernardini, Rossi and others (25-29,33) who find an exponential absorption with a coefficient of about 120 g/cm^2 of air. Studies of the absorption of the radiation producing photographic stars as well as direct measurements by this laboratory of the relative proton

intensity between 3.3 km and sea level gives similar absorption path lengths. It should be pointed out that an exponential absorption of this path length cannot hold to the top of the atmosphere, as in this case the observed proton intensity of 3.3 km. would be much too large as compared to the primary proton intensity at the top of the atmosphere. Instead (and there is some experimental evidence to the effect) it is probable that for the very high energy protons at the top of the atmosphere the effective removal path length is much larger due to the larger number of "generations" of secondaries of sufficient energy to continue the cascade. In the following treatment of the angular spread of the proton radiation a constant removal path length of 120 g/cm^2 is assumed. In making comparisons with observations made at 3.3 km., it is not necessary that this assumption hold to the top of the atmosphere, but rather that it be good from heights of 3.3 km. to sea level. Protons observed in this investigation lie principally between 0.5 Bev/c and 1.0 Bev/c. On the basis of ionization loss alone, these protons must have had momenta greater by some 2 Bev/c at the top of the atmosphere. As they will have undergone several nuclear collisions, the primary energy must have been several times greater than this. For protons of momenta above 7.5 Bev/c the primary distribution is isotropic above the horizon, as shown by the Lemaitre-

Vallarta theory (35) of the geomagnetic effect. It can be
expected then that the protons observed at 3.3 km. are
derived from an initially isotropic radiation. The radiation
at 3.3 km. then can be considered as the superposition of the
radiation due to equal contributions from each direction of
primary incidence. The observed angular spread at 3.3 km.
as well as absorption path lengths as measured for either the
total or vertical radiation depend in part on geometrical
factors resulting from this superposition of contributions
from many primary directions. It is the object of the fol-
lowing treatment to attempt to separate out the purely
geometrical factors and so arrive at an estimate of the
angular spread and absorption path length as determined by
the physical processes and cross-sections. It is clear, for
example, that a primary radiation all of vertical incidence
would not give rise to so great an angular spread at 3.3 km.
as that observed. Thus the observed angular spread repre-
sents an upper limit to that due to nuclear scattering in
traversing this absorber thickness. We attempt to obtain a
closer approximation to the angular spread due solely to the
nuclear scattering through the following assumptions:

1. The primary proton intensity is the same at all
   directions of incidence.

2. The intensity of secondaries at depth X due to
   primaries of zenith angle θ_0 (independent of

azimuth) depends only on the diagonal distance
d in g/cm^2 as measured along this zenith direction.

3. This intensity decreases exponentially with a path
length of 120 g/cm^2.

4. The angular spread of secondaries due to the primary
radiation in a given direction is represented by a
$\cos^n \omega$ law centered about this direction with n
independent of depth.

The first assumption is completely justified for primary
momenta above 7.5 Bev/c by the geomagnetic theory. As a
result of the following computation the assumption that the
primary radiation is isotropic for angles greater than 45°
is found unnecessary. For this smaller angle, geomagnetic
theory insures isotropy for momenta as low as 3.3 Bev/c.

The second assumption would be strictly true if one
neglected scattering. With scattering, the geometrical situa-
tion is not strictly the same for all zenith angles. A
primary traversing a given path near the top of the atmosphere
will produce secondaries at lower altitudes with large lateral
displacements from its original path. As compared to vertical
incidence, minimum path lengths for these secondaries (from
the point of observation to the top of the atmosphere) will
be increased for 180° of azimuth and correspondingly decreased
for the other 180°. Except for large zenith angles, since
average path lengths are the same, the situation will not

differ from that for vertical incidence.

Assumption three conforms to the large body of experimental determinations of this attenuation. While, as has been pointed out, this cannot hold to the top of the atmosphere, for the present purpose it need only be a close approximation for atmospheric depths from about 700 to 1000 g/cm^2. Experimental evidence indicates its validity below 60,000 feet (32).

In regard to assumption four, a $\cos^n \omega$ scattering law has no theoretical foundation. Its use conforms to usual practice, n being adjusted to give the experimentally determined rate of decrease. The assumption that n is constant cannot be true over large ranges of distance. Again this only need be approximately true over a range of 700 to 1000 g/cm^2. As n will be a function of the proton energies involved, similarity of the proton spectra at 700 and 1000 g/cm^2 can be taken as a measure of the constancy of n. Evidence for this has been provided by Wilson (21).

The physical problem involved here is similar to that considered in the Gross transformation (31), with the addition of the effects due to scattering. The additional complexity of the present situation necessitates resort to graphical methods.

Symbols to be used are defined as follows (see Figure VII for the coordinate system used).

$I_0 (\theta_o, \varphi_o)$ Differential proton intensity at the top of the atmosphere at spherical coordinates θ_o, φ_o in particles/Bev/c sterad cm^2 hour. This is assumed to be constant in θ_o and φ_o.

I_0 Total differential intensity at the top of the atmosphere $= \int_\Omega I_o(\theta_o,\varphi_o)\, d\Omega_o = 2\pi\, I_o(\theta_o,\varphi_o)$ particles/cm^2/Bev/c hour.

x   Depth of the point of observation measured in path lengths of 120 g/cm^2.

$I_x(\theta_o, \varphi_o, \theta_x, \varphi_x)$ Portion of the differential proton intensity at depth x observed at angles θ_x, φ_x contributed by the primary radiation incident at angles θ_o, φ_o at the top of the atmosphere, in particles/Bev/c cm^2 sterad^2 hour.

$I_x(\theta_x, \varphi_x)$ Differential proton intensity at depth x observed at angles θ_x, φ_x due to the contributions from all primary radiation, in particles/Bev/c cm^2 sterad hour.

ω Angle between $d\Omega_o$ and $d\Omega_x$. See Figure VIII.
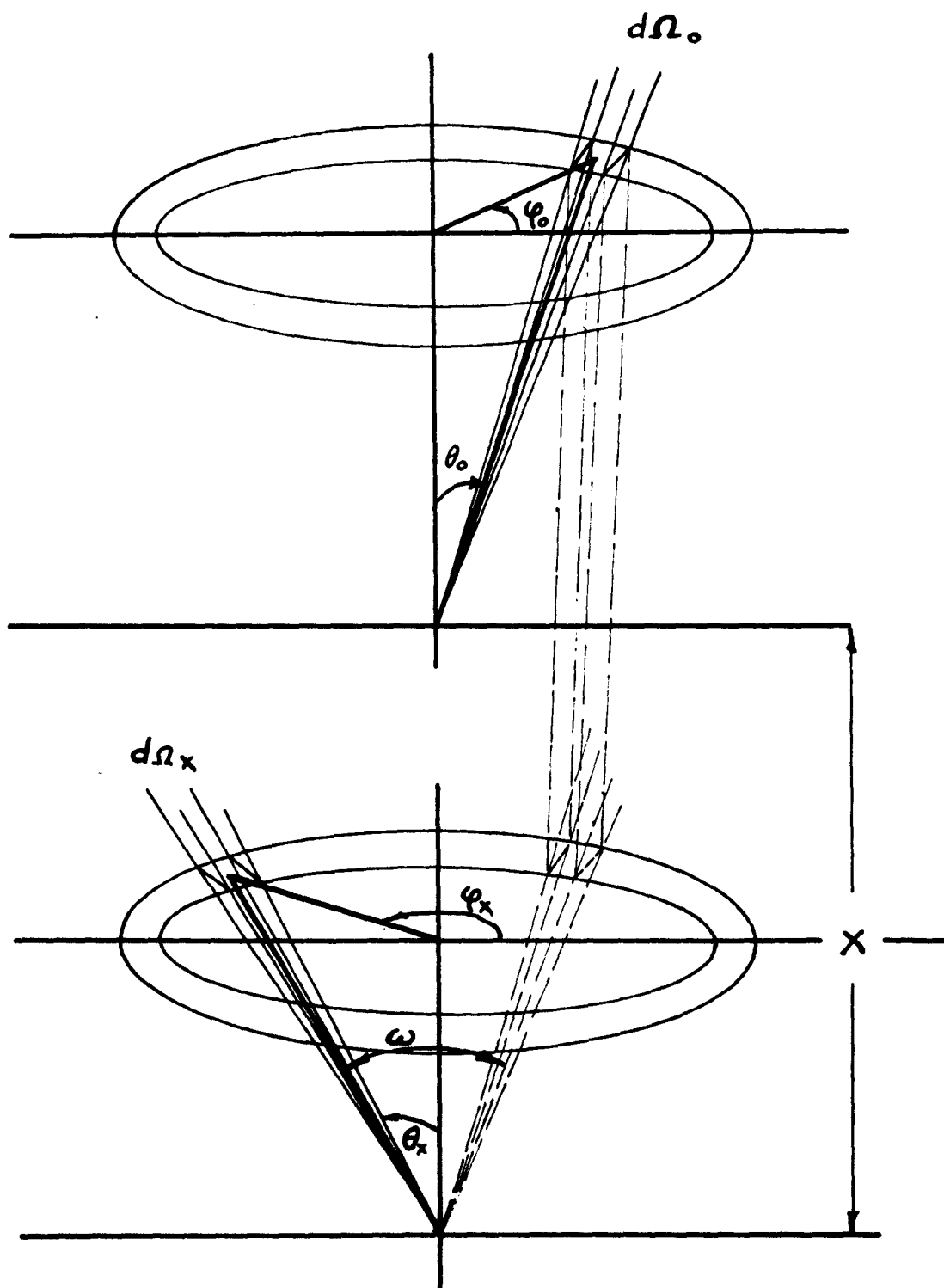
FIGURE VIII
SCHEMATIC DIAGRAM OF THE
COORDINATE SYSTEM USED

The counting rate of a Geiger counter telescope at the top of the atmosphere will be proportional to $I_0(\theta_0, \varphi_0)d\Omega_0$ where $d\Omega_0$ is the aperture of the telescope. The telescope at depth x will record $I_x(\theta_x, \varphi_x)d\Omega_x$. We wish to account for the fact that this latter rate falls by a factor of 3.2 from the vertical to $45°$ zenith angle. For this purpose we assume that

$$I_x(\theta_0, \varphi_0, \theta_x, \varphi_x) = kI_0(\theta_0, \varphi_0) e^{-\frac{x}{\cos\theta_0}} \cos^n\omega$$

We quickly find from Figure VIII that

$$\cos\omega = \sin\theta_0 \sin\theta_x \cos(\varphi_0 - \varphi_x) + \cos\theta_0 \cos\theta_x$$

so that $I_x(\theta_x, \varphi_x)d\Omega_x$

$$= \int_{\Omega_0} kI_0(\theta_0, \varphi_0) e^{-\frac{x}{\cos\theta_0}} \left[\cos\theta_0 \cos\theta_x + \sin\theta_0 \sin\theta_x \cos(\varphi_0 - \varphi_x)\right]^n d\Omega_0 d\Omega_x$$

where k is a normalizing factor and Ω_0 is the upper hemisphere. The determination of k can be made immediately by noticing that $\int_{\Omega_x} I_x(\theta_0, \varphi_0, \theta_x, \varphi_x)d\Omega_x$

$$= kI_0(\theta_0, \varphi_0) e^{-\frac{x}{\cos\theta_0}} \int_{\Omega_x} \cos^n\omega \, d\Omega_x \, d\Omega_0$$

must reduce to $I_0(\theta_0, \varphi_0)d\Omega_0$ for the case of no absorption, i.e., infinite removal path length. This means that x is zero and the exponential factor is unity. Thus from

$$k\int_{\Omega_x} \left[\cos\theta_0 \cos\theta_x + \sin\theta_0 \sin\theta_x \cos(\varphi_0 - \varphi_x)\right]^n d\Omega_x = 1$$

where Ω_x is again the upper hemisphere, k can presumably be found. The result, however, evidently depends on θ_o. This is to be expected, since for larger values of θ_o, the $\cos^n\omega$ distribution places particles outside the limits of integration. However, it will be shown immediately below that the exponent n is large enough so that the contributions to the above integral for values of θ_x greater than 90° are negligibly small for θ_o less than 45°, which is the region of interest. Thus it is legitimate to set $\theta_o = 0$, with the result

$$k \int_0^{\frac{\pi}{2}} \int_0^{2\pi} \cos^n\theta_x \, \sin\theta_x \, d\varphi_x \, d\theta_x = 1$$

$$2\pi k \int_0^{\frac{\pi}{2}} \cos^n\theta_x \, d(\cos\theta_x) = 1$$

or $\quad k = \dfrac{n+1}{2\pi}$

The determination of n is independent of this result.

Involved in the choice of the $\cos^n\omega$ dependence for an assumed scattering distribution is the fact that forward scattering predominates and that scattering in excess of 90° is negligibly small. Since $\cos^n\omega$ vanishes at 90°, the behavior of the forward scattering is fairly well approximated. However, $\cos^n\omega$ is not zero beyond 90°, and contributions to the integral will occur unless appropriate limits for the integration are defined. Hence, the integration will extend only over that portion of the upper hemisphere containing

directional rays making an angle less than or equal to $90°$ with the direction defined by θ_X . It will be shown later that this limitation is unimportant. The physical situation demands that we have axial symmetry about the vertical (no deflection by the earth's magnetic field is assumed), and hence, the result must be independent of φ_X . This allows the choice $\varphi_X = 0$. Thus the region of integration depends only on θ_X , and is shown in Figure IX. The shape of the region of integration shows that if the coordinates θ_0 , φ_0 are retained, the limits of integration over φ_0 will be functions of θ_0. To avoid this complication, a change of coordinates is in order. This is shown in Figure X. The transformed integral is then of the form. $I_X(\theta_X, \varphi_X) d\Omega_X$

$$= k I_0(\theta_0, \varphi_0) \int_0^{\frac{\pi}{2}+\alpha} \cos^n(\xi - \alpha) \int_0^\pi e^{-\frac{x}{\sin\lambda \sin\xi}} \sin^{n+1}\lambda \, d\lambda \, d\xi \, d\Omega_X$$

where $\alpha = \frac{\pi}{2} - \theta_X$.

We have data on this quantity for two directions of observation, hence the integration will be performed for just these two values, as it must be carried out graphically.

The object of the computation, of course, is to find n. The values of $I_X(0, \varphi_X)$ and $I_X(\frac{\pi}{4}, \varphi_X)$ have been obtained for n = 5, 6 and 7 at x = 5.4 corresponding to an atmospheric depth of 650 g/cm^2 = 3.3 km. altitude. These are shown in Table V together with the ratios $\rho = I_X(0, \varphi_X)$
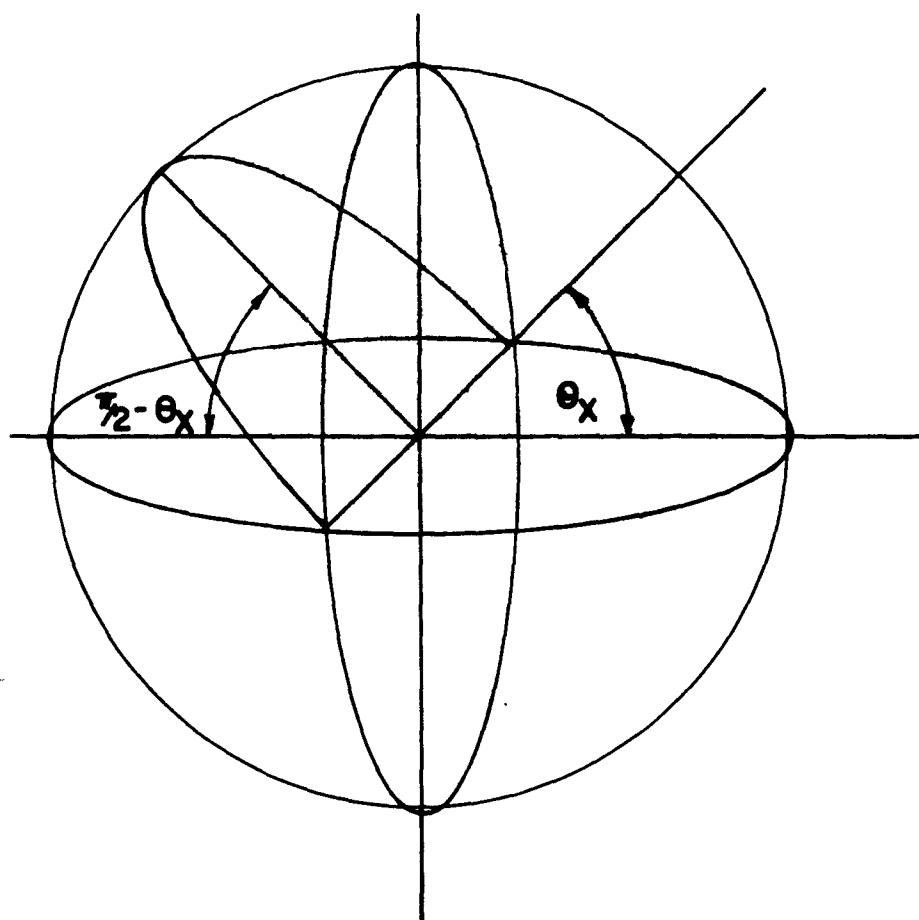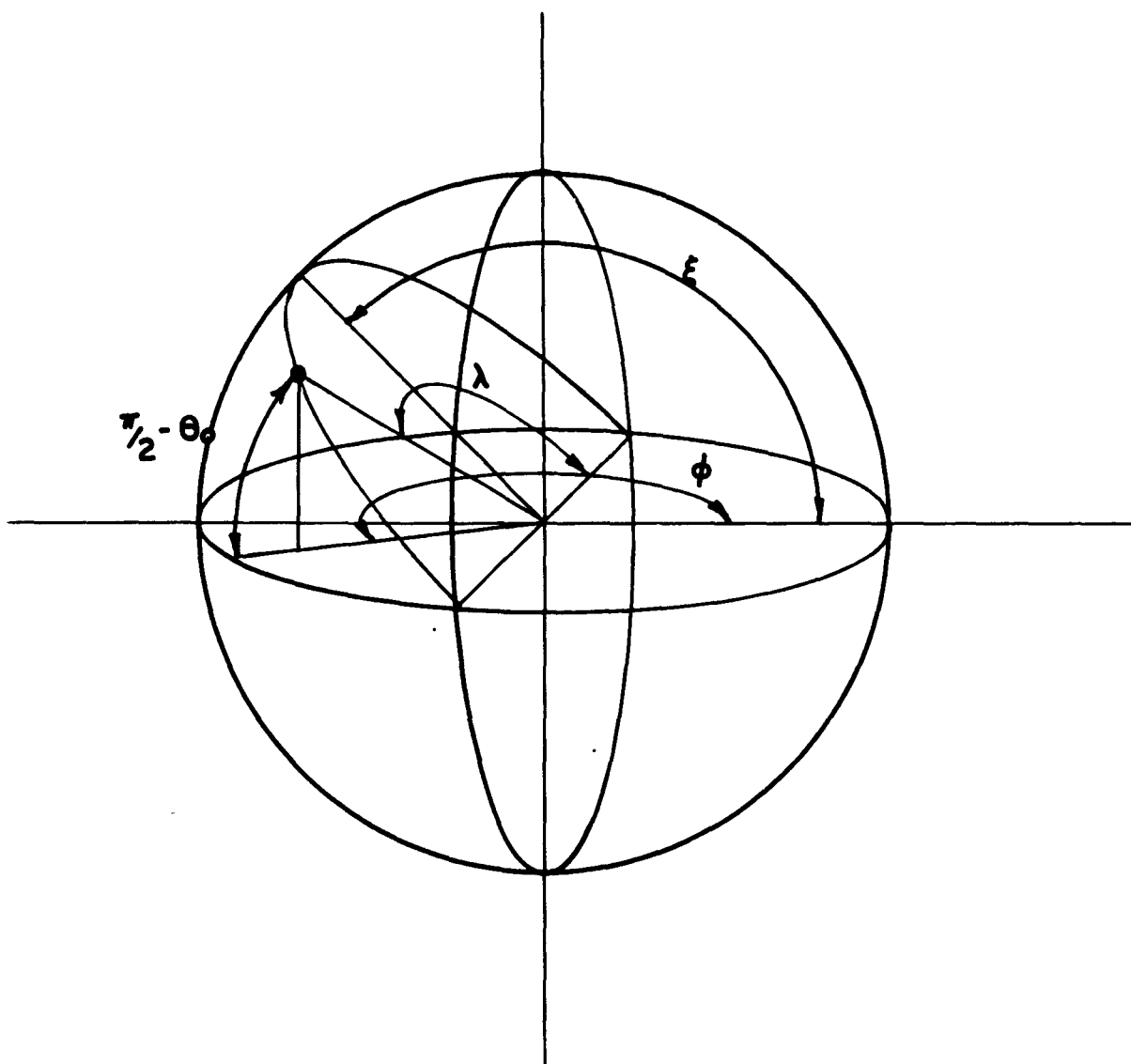
FIGURE IX
REGION OF INTEGRATION

FIGURE X
SKETCH OF THE
NEW COODINATE SYSTEM

$/I_x(\frac{\pi}{4}, \varphi_x)$ which are the measured quantities under discussion. It is seen that ρ is a fairly sensitive function of n, and that by interpolating, n can be assigned the value 6.5. Also included in the table is the value of ρ for n equal to "infinity," i.e., assuming no scattering whatsoever and that ρ is simply given by $\rho = e^{-\frac{x - x'}{L}}$ where x' is the distance to the top of the atmosphere along the diagonal ray at 45° zenith angle to the vertical.

The value of n so determined is dependent on the choice of path length. The sensitivity of the dependence is not great. The figure for the path length as determined by this laboratory is 125 ± 8 g/cm^2. Other values (29) are more closely centered about 120 g/cm^2. Values from nuclear plate data (26) are somewhat higher (about 135 g/cm^2), but refer to particles in much broader momentum bands. Within the region L = 100 to 140 g/cm^2, n varies from 6.0 to 8.5. Within the region L = 125 ± 8 g/cm^2, and within the statistical accuracy of the experimental value of ρ, n has the value 6.5 ± 0.7.

The value ρ = 3.2 is thus shown to be the result of an effective scattering distribution of $\cos^{6.5}\omega$. This is a fairly sharp distribution, falling off by a factor of nine from zero to 45 degrees zenith angle. It is of no small interest then that the use of such a distribution has the effect of reducing the value of ρ by a factor greater than three. The effect of scattering, however, must be included,

since the observed zenith angle dependence could be obtained purely from attenuation considerations only for path lengths in excess of 300 g/cm^2.

The behavior of the integrand of the above integral shows that the contribution to the vertical radiation at depth x from the primary radiation incident at angles greater than 45 degrees is entirely negligible (less than 0.1% for all values of n greater than 5), and contributions from the same source to the radiation observed at 45° at depth x is quite small (less than 5% for n greater than 5), primarily as a result of the exponential factor. This provides the justification for the assumed isotropy of the primary radiation, since lack of isotropy at zenith angles greater than 45° will have no effect on the computed values of $I_x(0, \varphi_x)$ and $I_x(\frac{\pi}{4}, \varphi_x)$. Hence, we need justify an assumed isotropy only at angles less than 45° within which protons are isotropic at momenta as low as 3.3 Bev/c, according to the Lemaitre-Vallarta theory.

Knowledge of the normalization factor allows one to compute an effective path length for removal which takes into account the scattering factor. Thus the computed ratio

$$\frac{I_0(0, \varphi_0)}{I_x(0, \varphi_x)}$$

(both in the vertical direction) represents the actual measured

ratio of intensities at 650 and zero g/cm^2 depths respectively, and when equated to $\exp(-650/L)$ yields the measured value of L. These ratios are exhibited in Table V for n = 5, 6,7 and infinity, as well as the associated values for L. These effective values of L are all somewhat smaller than 120 g/cm^2, as is expected, since more particles are scattered out of the vertical beam than into it, thus increasing the apparent attenuation of the vertical beam.

TABLE V

INTENSITY RATIOS AND EFFECTIVE PATH LENGTHS

n	$I_x(0, \varphi_x)$	$I_x(\frac{\pi}{4}, \varphi_x)$	$= \frac{I_x(0, \varphi_x)}{I_x(\frac{\pi}{4}, \varphi_x)}$	"Effective" Path Length
5	$2.28 \times 10^{-3} I_0$	$.857 \times 10^{-3} I_0$	2.66	106.5 gm/cm^2
6	$2.46 \times 10^{-3} I_0$	$.840 \times 10^{-3} I_0$	2.93	108 "
7	$2.65 \times 10^{-3} I_0$	$.755 \times 10^{-3} I_0$	3.51	109 "
Inf.	$4.53 \times 10^{-3} I_0$	$.465 \times 10^{-3} I_0$	9.70	120 "

As mentioned before, the exponential factor is responsible for the sharp cutoff at angles in the vicinity of 30-45 degrees. As one goes to greater and greater depths, i.e., to larger values of x, the sharpness of the cutoff will be increased somewhat (in addition to the larger attenuation) so that at sea level the result of a computation of the ratio

of the vertical intensity to the 45° intensity is about 3.5.
There is no experimental verification of this surmise. The
extreme difficulty of picking up any protons at all at sea
level (about 1% of the total penetrating component) indicates
that a statistically meaningful determination of this ratio
would require a long and careful but not impractical measure-
ment.

As mentioned in the introduction, the above result
places an upper limit on the average deflection suffered by
a proton in a nuclear collision. It was found that the intro-
duction of a $\cos^{6.5}\omega$ scattering distribution yielded a satis-
factory result for the gross zenith angle dependence. A
proton traversing the distance from the top of the atmosphere
to 3.3 km. will undergo on the average 10 collisions. This
corresponds to the geometrical cross-section rather than the
removal path length used above. Its use has been justified
by Heitler and Janossy (14). Such protons are extremely rare,
of course, since they have a path length for removal of only
twice the distance corresponding to the geometrical cross-
section. But it makes no difference whether one considers a
single proton which retains its identity throughout the ten
collisions or whether one asks for the total angle that the
final descendant makes with the original primary after ten
"generations," the latter situation being far more likely. It
is permissible, therefore, to consider a single proton.

If we assume that each proton suffers exactly ten collisions, and that after each collision the new direction differs from the old by an angle of exactly $\pm \alpha$, a unique distribution after the tenth encounter is determined, which depends only on α. Since $\cos^{6.5}\omega$ was introduced artificially there is no justification for asking that this statistical distribution coincide with it. One can, however, compare the integrals of the two distributions, i.e. ask for the angle for which the particle, after ten encounters, suffers a total angular deflection of less than, say, twenty degrees, with a certain probability computable from the $\cos^{6.5}\omega$ distribution. This problem in three dimensions, despite its similarity to the "random walk" problems of mathematical statistics, and its simplifying assumptions, is of enormous complexity, an unfortunate characteristic of plural scattering problems.

The two-dimensional problem, corresponding to the projection of the three dimensional scattering distribution on a vertical plane, is simpler, and actually corresponds to what is observed in this experiment. This two dimensional distribution predicts that about 60% of the particles make angles of less than 20 degrees with the primary direction. The problem then is to adjust α so that the statistical distribution indicates the same thing. The choice of 20 degrees as the matching point is convenient, for it is close to the half value point of the distribtuion. The percentage

for a given matching angle is given by another graphical
integration, hence it is not convenient to match at the exact
angle within which exactly half the particles are scattered,
as its determination is unnecessarily laborious. Angles
giving percentages far removed from 50% are not expected to
give the most accurate matching since at small angles the
projected $\cos^{6.5} \omega$ distribution is too slowly varying, while
at large angles the statistical distribution is too crude.

In a single scattering, it is assumed that a particle
is deflected through an angle of $\pm \alpha$ and that the ten
encounters are statistically independent. Then there are 2^{10}
possible trajectories, corresponding to six distinct total
angular deflections. These deflections, along with their
relative probabilities, are enumerated in Table VI. One finds
that a total scattering angle of about 4α corresponds to a
probability of about 60%. Hence from $4\alpha = 20°$, one gets
$\alpha = 5°$.

A check of this figure may be had by noticing that a
proton's behavior is similar to a simple diffusion process.
The root-mean-square total deviation of a proton undergoing
N encounters with a scattering angle of α per encounter is
given by

$$\bar{A} = \sqrt{\langle A^2 \rangle} = \sqrt{N} \ \alpha.$$

With $\bar{A}$ roughly equal to $20°$ as before, and with ten encounters,

$$\alpha = 20/\sqrt{10} = 6.3°$$

which compares with the previous result, but the smallness of N limits the accuracy of α.

Thus a model of the scattering process has been constructed which gives a result roughly approximating the observed distribution. Present data do not warrant a more detailed analysis.

TABLE VI

SIMPLE TWO-DIMENSIONAL SCATTERING PROBABILITIES

θ	Relative Probability of Scattering at Angle θ	Probability That a Particle Be Scattered Through an Angle Less Than θ
90°	0	1.0000
10	2	0.9981
8	20	0.9785
6	90	0.8906
4	240	0.6563
2	420	0.2461
0	252	0.0000

Total = 1024 = 2^{10}

CHAPTER VI

COMPARISON WITH THE RESULTS OF OTHER AUTHORS

The only published data at all concerned with the problem treated here is the work of Walker (33) and Branch (36). Walker performed a counter-absorber type of experiment at 3.26 km. elevation and at sea level in which recorded events are those due to charged particles producing penetrating showers in blocks of lead absorber of varying thicknesses. After elaborate precautions to remove the soft and the mesonic components, he is able to call such particles protons, but the method of selection only vaguely defines accepted momentum. Walker's requirements for the lowest energy case are that a charged particle traverse two trays of counters separated by 12 inches, enter an 8-inch block of lead, and produce a shower there, whose presence shall be indicated by the discharge of three or more counters in a tray located below the absorber. Knowledge of which counters in the upper two trays were discharged yields the zenith angle dependence to 25° in six steps. The only limit that can be placed on the extent of the accepted momentum band is a lower one, which, because of the requirement for shower production, is certainly very much higher than the 1 Bev/c maximum cutoff for this experiment. This fact is further substantiated by Walker's ratio of the rate at elevation to that at sea level. This ratio is about

four, which is far removed from the well-established ratio of about twenty as obtained by this laboratory, by Wilson (21) and by Whittemore and Shutt (34), for low (less than 1 Bev/c) protons.

Walker finds that his data at elevation can best be correlated with a $\cos^n\theta$ distribution with n equal to 5.5 ± 0.7, while at sea level the exponent is 3.4 ± 1.0. The increase in exponent with altitude is not at all reasonable in the light of the model presented here. The sea level exponent agrees with the figure given in Chapter V, Section 2, but of course the agreement has little meaning as the data do not overlap. Similar work has been done by Brown and McKay (37).

Branch has determined the angular distribution about the shower axis of penetrating particles in extensive air showers. Such showers, of course, include, in addition to nucleons, many pi and mu mesons. A conclusion therefrom, relevant to this problem, is nevertheless possible, since Branch finds a root mean square angular deviation of emergent particles of about 3 degrees. This figure agrees fairly well with the figure 5° presented here. These two numbers are to be contrasted with the value 15-20 degrees which the early theoretical treatments by Messel et al (8-20) gave. Branch's result, which this experiment independently corroborates, has caused drastic changes in the nature of the assumed cross-section (38,39).

CHAPTER VII

SUMMARY

The proton spectrum for particles in the momentum band 0.4-1.0 Bev/c and the meson spectrum for particles in the momentum band 0.09-0.34 Bev/c at zenith angles 45° East, vertical, and 45° West, have been obtained at 3.3 km. elevation and magnetic latitude 48° North.

The behavior of the zenith angle dependence of mu-mesons has been found to be consistent with a transformation described by Charbonnier for higher energies, involving only the momentum loss by ionization of mesons at minimum ionization and the well-defined radioactive properties of this particle.

The zenith angle dependence of protons, along with a simplified phenomenological calculation of same, is presented as new data on the nucleonic cascade. Theoretical calculations presently found in the literature are not yet well enough founded to allow prediction of these data, nor have they been used to yield the differential momentum spectra of limited extent as presented here. It is found experimentally that the gross zenith angle dependence will fit a $\cos^{3.2}\theta$ distribution at 45 degrees East or West. The simplified calculation assumes that a unidirectional component of the primary radiation will: (1) suffer exponential absorption

along its original path with a path length for removal of
120 g/cm^2 of air, and (2) acquire an ultimate distribution
at 3.3 km. due to scattering fitting a $\cos^n\omega$ law, n being
an adjustable parameter.

It is found that a value of n of about 6.5 yields a
unidirectional distribution which, when integrated over all
angles, results in a gross zenith angle dependence agreeing
with $\cos^{3.2}\theta$. The $\cos^n\omega$ distribution with n equal to 6.5
is quite sharp and leads to the conclusion that the average
projected scattering angle per collision is only about 5
degrees.

BIBLIOGRAPHY

1 C. E. Miller, J. E. Henderson, G. R. Garrison, W. M. Sandstrom — Bull. Am. Phys. Soc., $\underline{26}$, 25, 1951

2 C. E. Miller, J. E. Henderson, D. S. Potter, Jay Todd, Jr., and A. W. Wotring — Phys. Rev., $\underline{79}$, 459, 1950

3 C. E. Miller, J. E. Henderson, D. S. Potter, and Jay Todd, Jr. — Phys. Rev., $\underline{84}$, 981, 1951

4 D. S. Potter, Doctoral Thesis — Univ. of Wash., 1951

5 Jay Todd, Jr., Doctoral Thesis — Univ. of Wash., 1951

6 F. M. Charbonnier, Doctoral Thesis — Univ. of Wash., 1952

7 G. R. Garrison, Doctoral Thesis — Univ. of Wash., 1952

8 H. Messel and D. M. Ritson — Proc. Phys. Soc., $\underline{A63}$, 1359, 1950

9 L. Janossy and H. Messel — Proc. Roy. Irish Acad., $\underline{A54}$, 245, 1951

10 L. Janossy and H. Messel — Proc. Roy. Irish Acad., $\underline{A54}$, 217, 1951

11 H. Messel — Proc. Roy. Irish Acad., $\underline{A54}$, 125, 1951

12 H. S. Green and H. Messel — Phys. Rev., $\underline{83}$, 842, 1951

13 H. S. Green and H. Messel — Phys. Rev., $\underline{85}$, 679, 1951

14 W. Heitler and L. Janossy — Proc. Phys. Soc., $\underline{A62}$, 374, 1949

15 H. Messel — Phys. Rev., $\underline{83}$, 21, 1951

16 H. Messel — Phys. Rev., $\underline{83}$, 26, 1951

17 H. Messel and H. S. Green — Phys. Rev., $\underline{83}$, 1279, 1951

18 H. Messel and H. S. Green — Phys. Rev., $\underline{87}$, 738, 1952

19 B. A. Chartres and H. Messel — Phys. Rev. $\underline{87}$, 748, 1952

20 H. Messel and R. B. Potts — Phys. Rev. $\underline{87}$, 759, 1952

21 M. G. Mylroi and J. G. Wilson — Proc. Phys. Soc., $\underline{A64}$, 417, 1951

22 S. B. Treiman — Phys. Rev., $\underline{86}$, 917, 1952

23 G. Cocconi, V. Cocconi-Tongiorgi, and M. Widgoff — Phys. Rev., $\underline{79}$, 768, 1950

24 M. Conversi — Phys. Rev., $\underline{79}$, 749, 1950

25 B. Rossi — Rev. Mod. Phys., $\underline{20}$, 537, 1948

26 G. Bernardini, G. Cortini, and M. Manfredini — Phys. Rev., $\underline{74}$, 1878, 1948

27 E. P. George and A. C. Jason — Nature, $\underline{160}$, 327, 1947
Nature, $\underline{161}$, 248, 1948

28 H. E. Tatel and J. A. Van Allen — Phys. Rev., $\underline{73}$, 87, 1948

29 J. Tinlot — Phys. Rev., $\underline{73}$, 1476, 1948
Phys. Rev., $\underline{74}$, 1197, 1948

30 D. J. X. Montgomery — Cosmic Ray Physics, Princeton University Press, 1949

31 E. P. Gross — Zeits. für Physik, $\underline{83}$, 214, 1933

32 M. Blau and H. Wambacher — Akad. Wiss. Wien, $\underline{IIA146}$, 623, 1937

33 W. D. Walker — Phys. Rev. $\underline{77}$, 686, 1950

34 W. L. Whittemore and R. P. Shutt — Phys. Rev. $\underline{86}$, 940, 1952

35 G. Lemaitre and M. S. Vallarta — Phys. Rev. $\underline{43}$, 87, 1933

36 G. M. Branch — Phys. Rev. $\underline{84}$, 147, 1951

37 W. W. Brown and A. S. McKay — Phys. Rev., $\underline{76}$, 1034, 1949

38 H. Messel and H. S. Green — Phys. Rev., $\underline{87}$, 378, 1952

39 H. S. Green, H. Messel, and B. A. Chartres — Phys. Rev., $\underline{88}$, 1277, 1952

Professional

Dr. W. F. G. Swann, Director
Bartol Research Foundation
Franklin Institute
Swarthmore, Pennsylvania

Prof. C. C. Lauritsen
Department of Physics
California Institute of Technology
Pasadena, California

Prof. C. D. Anderson
Department of Physics
California Institute of Technology
Pasadena, California

Prof. R. B. Brode
Department of Physics
University of California
Berkeley 4, California

Prof. E. O. Lawrence
Radiation Laboratory
University of California
Berkeley 4, California

Prof. J. R. Richardson
Department of Physics
University of California
(Los Angeles)
Los Angeles 24, California

Prof. E. C. Creutz
Department of Physics
Carnegie Institute of Technology
Schenley Park
Pittsburgh 13, Pennsylvania

Dr. M. A. Tuve
Department of Terrestrial Magnetism
Carnegie Institution of Washington
Washington, D. C.

Dr. R. S. Shankland
Case Institute of Technology
Department of Physics
University Circle
Cleveland 6, Ohio

Prof. S. K. Allison
Institute of Nuclear Studies
University of Chicago
Chicago, Illinois

Prof. J. Rainwater
Columbia University
Nevis Cyclotron Laboratories
P. O. Box 117
Irvington-on-Hudson, New York

Prof. R. R. Wilson
Laboratory of Nuclear Studies
Cornell University
Ithaca, New York

Prof. W. M. Nielson
Department of Physics
Duke University
Durham, North Carolina

Dr. Guy Suits
Research Laboratory
General Electric Company
Schenectady, New York

Dr. Zoltan Bay
Department of Physics
George Washington University
Washington, D. C.

Prof. N. F. Ramsey
Department of Physics
Harvard University
Cambridge, Massachusetts

Director
Nuclear Laboratory
Harvard University
Cambridge, Massachusetts

Prof. F. W. Loomis
Department of Physics
University of Illinois
Urbana, Illinois

Prof. A. C. G. Mitchell
Department of Physics
Indiana University
Bloomington, Indiana

Prof. J. A. Van Allen
Department of Physics
State University of Iowa
Iowa City, Iowa

2

Prof. J. D. Stranathan
Department of Physics
University of Kansas
Lawrence, Kansas

Prof. J. M. Cork
Department of Physics
University of Michigan
Ann Arbor, Michigan

Prof. W. E. Hazen
Department of Physics
University of Michigan
Ann Arbor, Michigan

Prof. J. H. Williams
Department of Physics
University of Minnesota
Minneapolis, Minnesota

Prof. E. P. Ney
Department of Physics
University of Minnesota
Minneapolis, Minnesota

Prof. Truman S. Gray
Servo-Mechanisms Laboratory
Massachusetts Institute of Technology
Cambridge 39, Massachusetts

Professor J. R. Zacharias. . . . .(2)
Laboratory for Nuclear Science and
Engineering
Massachusetts Institute of Technology
Cambridge 39, Massachusetts

Prof. S. A. Korff
Department of Physics
New York University
University Heights
New York 53, New York

Prof. B. Waldman
Nuclear Physics Laboratory
University of Notre Dame
Notre Dame, Indiana

Prof. J. N. Cooper
Department of Physics
Ohio State University
Columbus 10, Ohio

Prof. W. E. Stephens
Department of Physics
University of Pennsylvania
Philadelphia 4, Pennsylvania

Prof. A. J. Allen
Department of Physics
University of Pittsburgh
Pittsburgh, Pennsylvania

Prof. G. T. Reynolds
Department of Physics
Princeton University
Princeton, New Jersey

Prof. M. G. White
Department of Physics
Princeton University
Princeton, New Jersey

Prof. Leticia del Rosario
Department of Physics
Gobierno De Puerto Rico
Universidad De Puerto Rico
Rio Piedras
Puerto Rico

Prof. K. Lark-Horovitz
Department of Physics
Purdue University
Lafayette, Indiana

Prof. T. W. Bonner
Department of Physics
Rice Institute
Houston, Texas

Prof. R. E. Marshak
Department of Physics
University of Rochester
Rochester, New York

Prof. Charles A. Whitmer
Chairman, Department of Physics
Rutgers University
New Brunswick, New Jersey

Prof. E. L. Ginzton
Microwave Laboratory
Standford University
Palo Alto, California

Prof. F. Bloch
Department of Physics
Stanford University
Palo Alto, California

Prof. J. D. Trimmer
Department of Physics
University of Tennesse
Knoxville, Tennesse

Prof. A. L. Hughes
Department of Physics
Washington University
St. Louis, Missouri

Dr. J. W. Coltman
Research Laboratories
Westinghouse Electric Corporation
East Pittsburgh, Pennsylvania

Prof. R. D. Sard
Department of Physics
Washington University
St. Louis, Missouri

Prof. R. G. Herb
Department of Physics
University of Wisconsin
Madison 6, Wisconsin

Prof. J. H. Manley
Department of Physics
University of Washington
Seattle 5, Washington

Prof. W. W. Watson . . . . (2)
Department of Physics
Sloane Physics Laboratory
Yale University
New Haven, Connecticut

Governmental

Chief of Naval Research . . . . (2)
Attn: Nuclear Physics Branch
Navy Department
Washington 25, D. C.

Superintendent, Nucleonics Division
Naval Research Laboratory
Anacostia, Washington, D. C.

Director, Naval Research Laboratory (9)
Attn: Technical Information Officer
Washington 25, D. C.

Chief, Bureau of Ships
Attn: Code 390
Navy Department
Washington 25, D. C.

Director
Office of Naval Research
Chicago Branch Office
844 North Rush Street
Chicago 11, Illinois

Chief, Bureau of Ships
Attn. Code 330
Navy Department
Washington 25, D. C.

Director
Office of Naval Research
San Francisco Branch Office
801 Donahue Street
San Francisco 24, California

Chief, Bureau of Ordnance
Attn: Rem
Navy Department
Washington 25, D. C.

Chief, Bureau of Ordnance
Attn: Re9a
Navy Department
Washington 25, D. C.

Director
Office of Naval Research
New York Branch Office
346 Broadway
New York 13, New York

Chief, Bureau of Aeronautics
Attn: RS-5
Navy Department
Washington 25, D. C.

Director
Office of Naval Research
Pasadena Branch Office
1030 East Green Street
Pasadena 1, California

Chief, Bureau of Aeronautics
Attn: Technical Library
Navy Department
Washington 25, D. C.

Officer in Charge . . . .(10)
Office of Naval Research
Navy No. 100
Fleet Post Office
New York, New York

Commanding Officer
Naval Radiological Defense Laboratory
San Francisco Naval Shipyard
San Francisco 24, California

Chief of Naval Operations
Attn: Op 36
Navy Department
Washington 25, D. C.

Commander, U. S. Naval Ordnance Test
Station
Technical Library
Inyokern, China Lake, California

Commanding General
Air Force Cambridge Research Center
Attn: Geophysics Research Library
230 Albany Street
Cambridge 39, Massachusetts

Senior Scientific Advisor
Office of the Under Secretary
of the Army
Department of the Army
Washington 25, D. C.

Director, Research and Development
Division
General Staff
Department of the Army
Washington 25, D. C.

Chief, Physics Branch
U. S. Atomic Energy Commission
1901 Constitution Avenue, N. W.
Washington 25, D. C.

U. S. Atomic Energy Commission
Attn: Roland Anderson
Patent Branch
1901 Constitution Avenue, N. W.
Washington 25, D. C.

U. S. Atomic Energy Commission . . (4)
Library Branch
Technical Information Division, ORE
P. O. Box E
Oak Ridge, Tennessee

Oak Ridge National Laboratory
Attn: Head, Physics Division
P. O. Box P
Oak Ridge, Tennessee

Brookhaven National Laboratory
Attn: Dr. S. C. Stanford
Research Library
Upton, L. I., New York

Oak Ridge National Laboratory
Attn: Central Files
P. O. Box P
Oak Ridge, Tennesse

Argonne National Laboratory
Attn: Hoylande D. Young
P. O. Box 5207
Chicago 80, Illinois

Document Custodian
Los Alamos Scientific Laboratory
P. O. Box 1663
Los Alamos, New Mexico

Technical Information Group
General Electric Company
P. O. Box 100
Richland, Washington

Carbide and Carbon Chemical Division
(K-25 Plant)
Plant Records Department
Central Files (K-25)
P. O. Box P
Oak Ridge, Tennessee

Carbide and Carbon Chemical Division
(Y-12 Plant)
Central Reports & Information (Y-12)
P. O. Box P
Oak Ridge Tennessee

Ames Laboratory
Iowa State College
P. O. Box 14A, Station A
Ames, Iowa

Knolls Atomic Power Laboratory
Attn: Document Librarian
P. O. Box 1072
Schenectady, New York

Mound Laboratory
Attn: Dr. M. M. Haring
U. S. Atomic Energy Commission
P. O. Box 32
Miamisburg, Ohio

Sandia Corporation
Sandia Base
Attn: Mr. Dale N. Evans
Classified Document Division
Albuquerque, New Mexico

U. S. Atomic Energy Commission
Attn: Division of Technical Information
     and Declassification Service
New York Operations Office
P. O. Box 30
Ansonia Station
New York 23, New York

National Bureau of Standards Library
Room 203, Northwest Building
Washington 25, D. C.

National Science Foundation
2144 California Street
Washington 25, D. C.

Commanding General
Air Research & Development Command
Attn: RDRRP
P. O. Box 1359
Baltimore 3, Maryland

Director, Office of Ordnance Research
2127 Myrtle Drive
Durham, North Carolina

Director
Office of Naval Research
Boston Branch Office
150 Causeway Street
Boston, Massachusetts

Foreign

Doctor Cesar Lattes
Scientific Director, Brazilian Center
of Physical Research
Rio de Janeiro, Brazil